Spring 2016

Photophysical Characterization of Luminophores for Use in Sensing Applications

Stephanie N. Kramer
Elizabethtown College

Photophysical Characterization of Luminophores for Use in Sensing Applications

By

Stephanie N. Kramer

This thesis is submitted in partial fulfillment of the requirements for Honors in the Discipline in Chemistry and the Elizabethtown College Honors Program.

Department of Chemistry & Biochemistry

Elizabethtown College

May 6, 2016

Elizabethtown College
Department of Chemistry & Biochemistry

The Thesis submitted by

Stephanie N. Kramer

under the title

"Photophysical Characterization of Luminophores for Use in Sensing Applications"

has been read and undersigned. It is hereby recommended for acceptance in partial fulfillment of the graduation requirements for Department Honors in Chemistry & Biochemistry

_____ _____
(Signed) Thomas E. Hagan, Jr. (Date)

_____ _____
(Signed) Gary G. Hoffman (Date)

_____ _____
(Signed) Kristi A. Kneas (Date)
Research Advisor

_____ _____
(Signed) James A. MacKay (Date)

_____ _____
(Signed) Jeffrey A. Rood (Date)

Recommendation accepted by the Chair of the Department of Chemistry & Biochemistry, Elizabethtown College:

_____
(Signed) Kristi A. Kneas

_____
(Date)

Abstract

Traditionally, in luminescence-based sensing, a sensor molecule is designed for one specific analyte. A new method of sensing was proposed which combines a non-luminescent sensing matrix and a luminescent reporter molecule that reacts to the change in its environment upon the interaction of the matrix with an analyte. In previous attempts at this method of sensing an environmentally-sensitive fluorophore was embedded into a hydrogel. However, leaching of the reporter molecule occurred with repeated use in aqueous phase sensing. In response to this limitation, two specific reporter molecules are explored: a nitrile derivative of dapoxyl sulfonic acid (compound **1**), which can be covalently bonded to the polymer support matrix and $[Os(CO)_2(sulf\text{-}dpp)Cl_2]$, which can be incorporated into a luminescent metal organic framework.

The solvent sensitivity of **1** was measured, and it was found that the derivative exhibits solvent-sensitivity, albeit complicated by the presence of two accessible excited states. The fluorophore was polymerized into an analyte-responsive hydrogel, and the sensitivity of the derivative to change in relative humidity was measured. It was found that the derivative lost some sensitivity when incorporated into the gel, though modified analyses of resultant data may allow for the emission responses to changes in polarity to be calibrated.

The viability of $[Os(CO)_2(sulf\text{-}dpp)Cl_2]$ as a reporter complex was determined. The quantum yield was found to be 0.00092 ± 0.00006 and the molar extinction coefficient was 410 ± 10 $L \cdot mol^{-1}cm^{-1}$ indicating that a fair amount of complex may be

necessary to provide reasonable sensor signal. However, if incorporated into a luminescent metal organic framework, the response might improve due to the increased rigidity of the environment of the complex.

Acknowledgments

I'd like to thank, first and foremost, my research advisor Dr. Kneas for all of the help she has given me throughout the year and for pushing me to complete the requirements of Honors in the Discipline. I would also like to thank Amy Wagner, John Tellis, and Chris Ryan: without these three, my project would not exist. I must also send a heartfelt thank you to the Elizabethtown Honors Program for providing the funding needed for me to travel to the national ACS meeting in San Diego where I had the opportunity to present my research.

Table of Contents

List of Tables

List of Figures

Introduction

Luminescence-based Sensing

Luminescence-based sensing is a measurement method that uses the radiation emitted from a molecule in an excited state for the purpose of detecting the presence, and often the amount, of a particular analyte.[1-5] This method of detection can be used for a variety of applications including measuring tumor oxygenation and detecting trace explosives.[6,7] For the measurement of tumor oxygenation, a fiber-optic sensor is used along with a compound whose luminescence is quenched by the presence of oxygen. The main measurement of these sensors is the oxygen-quenched excited state lifetime of the luminescent reporter molecule.[6] When detecting trace explosives, the analyte is tagged with europium complexes that display long-lived luminescence (0.4 ms), which is analyzed via time-resolved emission. Another method for detecting trace explosives is through the use of luminescent polymers. When the explosives bind to the polymer, the luminescence of the polymer exhibits a "turn-off" behavior; this has been shown to be an effective method for the detection of trinitrotoluene (TNT).[7,8,9]

Luminescence-based sensing is more sensitive compared to other analytical methods, having a detection limit 1-3 orders of magnitude lower than those of absorbance spectroscopy.[1] The selectivity of luminescence measurements is also excellent in comparison to other methods due to the fact that a limited number of known molecules will luminesce in the visible region of the electromagnetic spectrum, and these compounds can be used as reporters for a variety of analytes. While this selectivity is good and a variety of analytes can be measured, it is difficult to engineer new

luminescent reporter molecules to extend the range of possible analytes. Part of the focus of this research is to work towards the development a more versatile luminescence-based sensing approach.

Various luminescence properties of reporter molecules can be used in detection of analytes, such as emission wavelength, luminescence intensity, excited-state lifetime, and fluorescence anisotropy, causing luminescence-based methods to be attractive to researches attempting to further the development of highly sensitive and selective sensors.[5] Some of these properties (i.e. emission wavelength, fluorescence anisotropy) are independent of reporter concentration, detector sensitivity, and source intensity, which is particularly useful when calibrating reporter response. In some other cases, when these "sensing" molecules are exposed to the desired analyte, the emission wavelength and/or the intensity of that signal changes; the emission peak observed will shift towards higher wavelengths due to the decrease in energy while the intensity of the peak will generally decrease. The cause for the decrease in intensity is due to a variety of processes, two of which are collisional quenching and static quenching. Collisional quenching is when an excited fluorophore is deactivated when it comes in contact with the analyte. Static quenching occurs when electrons are shared between the sensor and the analyte, forming a non-emissive complex.[5]

Among the compounds used in luminescence-based sensors are luminescent inorganic TMCs and fluorescent organic dyes. In this body of work, the effect that local environment has on the luminescence of a particular class of TMCs and fluorescent

organic dyes will be investigated. The magnitude of this effect will have an inherent consequence on the sensing abilities and applications of the compounds studied.

Previously, among the most studied luminescence-based sensing methods were oxygen sensors based on the dynamic quenching of luminescent ruthenium complexes.[10-13] However, ruthenium complexes, such as $[Ru(dpp)_3]Cl_2$ (where dpp is 4,7-diphenyl-1,10-phenanthroline), have also been utilized in the sensing of relative humidity and pH.[5,14,15] To date, there has been fairly extensive research into the development of luminescent TMCs with ruthenium and osmium metal centers.[16-19] Due to the high photostability of these TMCs, as well as the inherent ability to tune the photophysical properties through ligand modifications, TMCs have dominated much of the luminescence-based sensing research. Nevertheless, luminescent TMCs are not without limitations, mainly in sensor design challenges when the analyte of interest is in either the aqueous or vapor phases; there are very few luminophores appropriate for these applications.[20] It is important to ensure that any novel TMCs exhibit high photostability, high luminescent quantum yield, and both long absorption and emission wavelengths, which improve the quality of the sensor overall. The better the photostability of the complex, the longer the sensor will last, while high quantum yield allows for less of the sensing complex to be needed since there is a greater ratio of emitted light relative to that which is absorbed. Longer absorption and emission wavelengths limit the interference of autofluorescence, or the natural emission of light by biological structures, which can present a problem in biological applications.[21,22]

When compared to organic fluorescent dyes, TMCs exhibit longer excited-state lifetimes, defined as the average time a molecule remains in an excited state, and larger Stokes shifts, which is the difference in emission and excitation maxima.[5] In sensing, long excited-state lifetimes increase the sensitivity of the sensor, while large Stokes shifts lessen the chance that the emission and excitation peaks will overlap.[5] These two characteristics for luminescent TMCs are what make these complexes attractive as reporter molecules within luminescence-based sensors. Another trait exhibited by the TMCs is rigidochromism, which is the complexes' ability to change the emission wavelength due to the rigidity of the local environment. With an increase in the rigidity of the environment, there is an increase in the energy of the system, destabilizing the excited state and causing a blue-shift to be observed.[23] An increase in rigidity also inhibits some nonradiative deactivation pathways, thereby increasing the quantum yield of the complex.[18] Given that the eventual goal with the TMCs is to incorporate the complexes into a metal organic framework (MOF), which is a porous, extended structure comprised of metal ions coordinated to organic molecules, it is important to ensure that the complex is as photochemically stable as possible in the aqueous phase. This is accomplished by ensuring that the lowest excited state is either a CT or $\pi \rightarrow \pi^*$ and that the $d \rightarrow d$ state is well above the lowest energy excited state, thus preventing photochemical instability. Environment sensitivity is also an important characteristic for the complex. [16]

While most organic fluorescent dyes display shorter excited-state lifetimes and smaller Stokes shifts relative to the luminescent TMCs, there are some such as dapoxyl sulfonic acid (DSA) that actually exhibit very high quantum yield and larger Stokes shifts

which tend to make up for the short excited-state lifetime, shorter absorption and emission wavelengths, and poorer photostability. Unlike the TMCs, which can be easily modified, organic dyes suffer a greater hindrance when it comes to modification given that the emission of organic fluorophores is more sensitive to even very subtle changes in electronic structure.[24,25] An explicit example of this sensitivity can be seen in the work of Otsuki *et al.* in which the luminescent sensing ability of 5-dimethylamino-1-naphthalenesulfonic acid and 5-dimethylamino-1-naphthalenesulfonamide were compared. The limited structural difference between the two molecules caused a difference in maximum emission wavelengths of approximately 3000 nm.[26]

What is attractive about these organic molecules, though, specifically DSA and any related derivatives, is the extreme solvatochromic emission response. Solvatochromism is the ability of a chemical substance to exhibit an emission color change with varying polarity of the solvent environment. The key characteristics of these types of fluorescent organic dyes cause the sensors to function less on the physical interaction of the molecule with the analyte, like the luminescent TMCs previously mentioned, and more on the effect of the local environment.[5]

In past research, the solvatochromism of DSA was utilized for sensing purposes. Using the method described by Tellis *et al.*, the fluorescent compound acted as the reporter molecule within a smart hydrogel, which is a polymer that can experience reversible volume transitions upon exposure to a particular analyte (i.e. the gel will swell and contract with the introduction of analyte).[27,28] These gels were used in relative humidity sensing and exhibited reasonable sensitivity, as shown in Figure 1, with the

shift in emission to longer wavelengths upon increase in relative humidity. However, once the gels were applied to aqueous phase sensing for measurement of lactate, it was found that the DSA started to leach out with continual use.

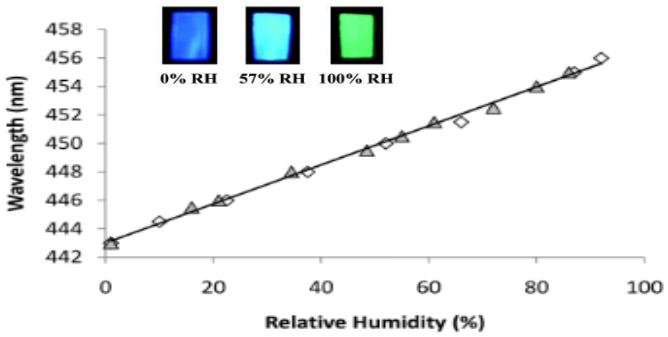

Figure 1: Emission wavelength as a function of relative humidity.[27]

The use of luminophores in sensing applications is a promising field in chemistry given the varying applications these compounds can be utilized for, including the previously mentioned relative humidity sensing and oxygen sensing, but also lactate sensing. While a variety of luminescence-based sensors do exist currently, there are still limitations in the application of these sensors. The main issue is the need for a luminescent reporter molecule for each analyte, so it is proposed that a non-luminescent, analyte-responsive sensing matrix would be developed and a luminescent reporter molecule would then be incorporated into the matrix. As previously mentioned, another limitation is in aqueous phase sensing. This calls for the preparation of novel luminophores designed to overcome this limitation in aqueous phase sensing. The general response to the observed leaching of the luminescent reporter molecule is to incorporate the reporter molecule directly into the matrix itself.

Fluorescent Organic Dyes for Sensing

The first organic fluorescent dye being studied for this research is the sodium salt of dapoxyl sulfonic acid (DSA) which can be seen in Figure 2.

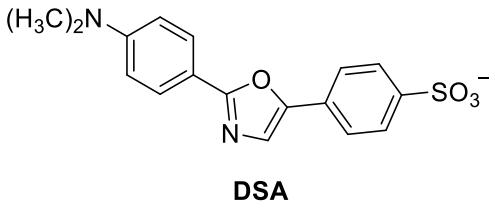

Figure 2: Structure of DSA.

As mentioned, these dyes were chosen for their high quantum yields, large Stokes shift, solubility in water, and their solvent sensitivity. The extreme solvent sensitivity and resulting Stokes shifts make DSA and its derivatives attractive for application in smart hydrogel sensors.[27] The inherent solvent sensitivity of the DSA molecule is especially important to this body of work. This sensitivity causes a noticeable red-shift in the emission wavelength, as well as a decrease in the emission intensity, with an increase in solvent polarity. A general depiction of this effect can be seen in Figure 3.

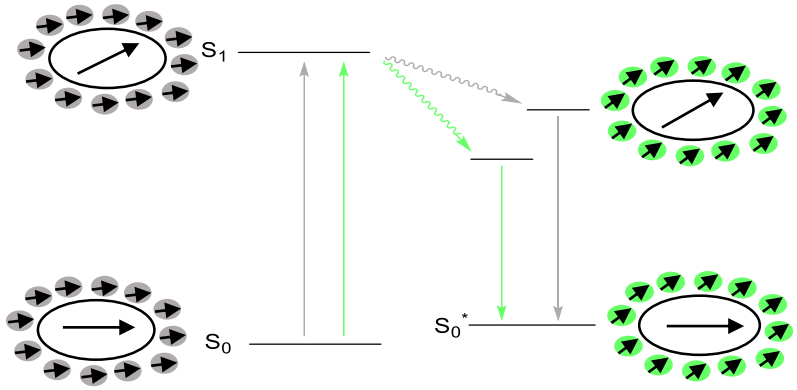

Figure 3: General energy level diagram depicting solvent sensitivity of a polar compound (white). Gray and green correspond to slightly polar solvent and highly polar molecules, respectively.

When exposed to radiation, fluorophores usually get excited to one of the vibrational levels within the first singlet state, S_1. The excess vibrational energy is quickly lost in the surrounding solvent. If the molecule is excited to the second singlet state, S_2, it will rapidly decay back down to the S_1 state due to internal conversion. The solvent environment can stabilize the excited singlet states of the fluorophore through the polar molecules present within the solvent, causing the energy of the system to decrease, thus resulting in a red-shift of the emission peak of the fluorophore. This typically occurs because the fluorophore has a larger dipole moment in an excited state than when in the ground state. The resulting emission that occurs is too rapid for the solvent molecules to reorient in the ground state so a higher energy ground state (denoted S_0^*) is entered, which also contributes to the observed shift in the emission to longer wavelengths. When an excited molecule is exposed to a non-polar environment, this stabilization is not possible, so the emission energy is higher and the wavelength is shorter. However, in general, this sensitivity to solvent polarity is only seen in fluorophores that are themselves polar since non-polar fluorophores do not exhibit as much sensitivity to any change in solvent polarity.[5] DSA is a highly polar molecule, causing it to be an attractive subject for study in solvent sensitivity measurements. General solvent trends are observed for DSA, which has a large dipole moment in the ground state (Figure 4).

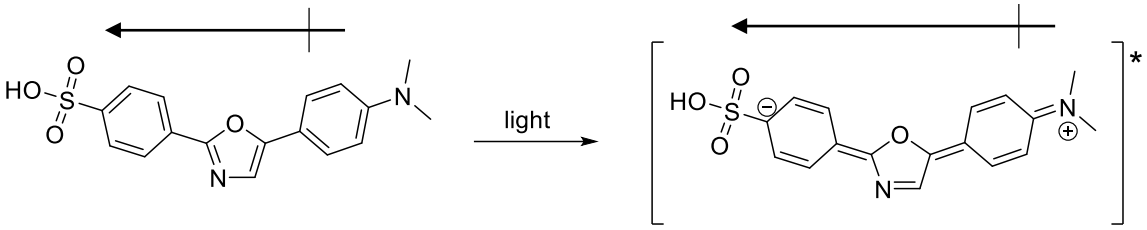

Figure 4: Relative change in the dipole of DSA when transitioning from the grounds state to an excited state.

The resulting solvent effect is even more significant in DSA because it also exhibits an intramolecular charge transfer (ICT) state as well as the charge separation in the excited state. This state can occur when a fluorophore contains both electron-accepting and electron-donating groups. An increase in charge separation within the molecule can occur after excitation. If the fluorophore is in a polar solvent environment, then the ICT state may be the lowest energy state of the fluorophore. This is due to the fact that the solvent will not only lower the energy of the excitation states, but it can also affect which state will be the lowest energy state of the fluorophore. In certain cases, in order to form the ICT, the molecule would need to rotate the groups, thus allowing a twisted internal charge transfer (TICT).[5] The DSA molecule has the ability to form ICT and TICT states which also contribute to the attractiveness of the fluorophore and its derivatives for solvent sensitivity measurements.

Extreme sensitivity to the polarity of its local environment makes DSA a sensitive reporter molecule in hydrogel-based sensors. When the smart hydrogel is contracted, thus less water is present, DSA experiences a more hydrophobic environment. But, with increase in analyte concentration, and influx of solvent, the hydrogel swells, and the fluorescent reporter molecule experiences a more polar environment and a concomitant

change in observed emission wavelength and intensity. However, DSA is limited in its sensing ability, mainly when incorporated into a hydrogel intended for aqueous phase sensing due to leaching. In order to circumvent the leaching of the reporter molecule from the gel, the MacKay research group designed and synthesized compound **1**. The goal of this design was to maintain the fluorescent DSA core, as well as the push-pull electronics of the original dye, but to also allow for the covalent attachment of the dye to the hydrogel. The addition of an acrylamide group was predicted to allow for this attachment to the hydrogel itself via polymerization, preventing the leaching from occurring. The resulting structure is shown in Figure 5.

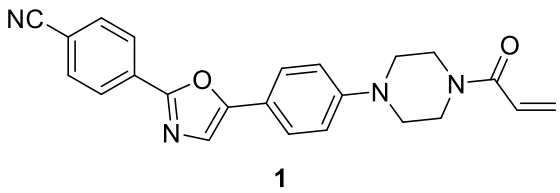

1

Figure 5: Structure of the nitrile DSA derivate (compound **1**).

In order to investigate the solvent sensitivity of the DSA dyes, an adaptation of the study of a DSA derivative by Diwu *et al.* was performed. In his experimentation, Diwu analyzed the solvent sensitivity of the DSA derivative, shown in Figure 6, by measuring the excitation and the emission spectra of the derivative in solvents of various polarities, as determined by the $E_T(30)$ polarity scale, and then calculating the Stokes shift for each environment.[29]

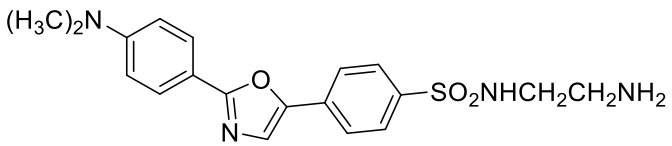

Figure 6: Structure of DSA derivative synthesized by Diwu *et al.*

This data was then analyzed by creating a Lippert plot, which is a plot of the Stokes shift versus the solvent polarity.[30] In this current work, the method employed by Diwu was utilized in order to measure the solvent effect on DSA and **1**. This was accomplished by dissolving the fluorophores in solvents of varying polarity and then measuring the Stokes shift for the compound in each solvent. The data obtained from this analysis, along with the data collected by Diwu, provided the baseline for the analysis of **1**. It was predicted that the polarity-sensitive DSA dyes would be appreciably solvent-dependent since an increase in environment polarity would result in an increase in the stabilization of the excited state. This increase in stabilization would decrease the energy of the excited state and increase the resulting emission wavelength.

Luminescent Transition Metal Complex for Sensing

Due to the limitations observed in the use of the DSA-embedded smart hydrogel in aqueous sensing, the use of luminescent MOFs as aqueous phase sensors was also explored. The specific TMC being studied for this research is $[Os(CO)_2(sulf\text{-}dpp)Cl_2]$ (where sulf-dpp is sulfonated 4,7-diphenyl-1,10-phenanthroline), Figure 7. In past studies by Baca *et al.*, $[Os(phen)(CN)_4]^{2-}$ produced appreciable signal due to the rigidity of the

phenanthroline ligand.[18] Since sulf-dpp is also a rigid ligand similar to phenanthroline, it was reasonable to predict that the signal produced by $[Os(CO)_2(sulf\text{-}dpp)Cl_2]$ would be appreciable.

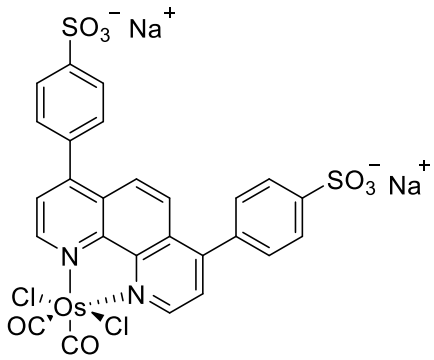

Figure 7: Structure of $[Os(CO)_2(sulf\text{-}dpp)Cl_2]$.

The research in the development of osmium as the metal center of a TMC capable of being used as a viable luminescence-based reporter molecule in a MOF is significant because, overall, osmium sensors are more photochemically robust than the ruthenium analogues due to the larger energy gap between the excited emitting state, MLCT, and the photochemically destructive higher energy states, d→d (Figure 8).[16]

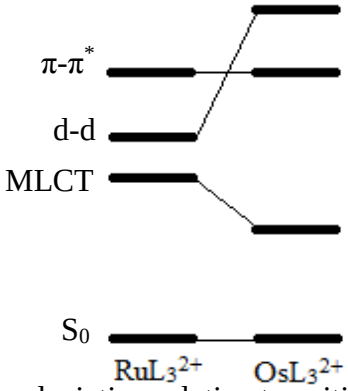

Figure 8: Simplified diagram depicting relative transition energies of the lowest triplet state ordering for a general ruthenium (II) complex and its analogous osmium (II) complex.[16]

These sensors also demonstrate modest red absorption, meaning that they can be excited with low-cost high-intensity red diode lasers. Unfortunately, when characterized in solution, osmium complexes exhibit shorter excited state lifetimes and smaller quantum yields compared to ruthenium complexes, as well as smaller intensities.[17,19] This shortening of the excited state lifetime is caused by what would appear at first to be an advantage of osmium over ruthenium: the increased splitting between the d→d and MLCT states due to the increase in spin-orbit coupling. Because osmium is easier to oxidize than ruthenium, the energy of the MLCT states is lowered, lengthening the gap between these states and the d→d. However, the MLCT state is so low that direct raditionless decay is more likely to occur, as per the energy gap law, reducing the lifetime of the osmium to approximately 50 ns versus the ruthenium's 600ns when comparing $[Os(bpy)]_3^{2+}$ and $[Ru(bpy)]_3^{2+}$ (where bpy is 2,2'-bipyridine).[16] The quantum yields are impacted by the heavy atom effect; the quantum yield is smaller as a result of there being less energy for emission due to an increase in the energy of the d-orbitals of the osmium atom.[17,18,19] In order to determine if $[Os(CO)_2(sulf\text{-}dpp)Cl_2]$ could be a useful luminescent reporter molecule, the quantum yield of the complex needed to be measured.

A procedure established by Horiba was used to determine the quantum yield of $[Os(CO)_2(sulf\text{-}dpp)Cl_2]$. This method includes choosing well characterized standards that absorb near a set excitation wavelength and emit in a region as the compound whose quantum yield is being measured. Each solution should not exceed a 0.1 absorbance at the excitation wavelength; this minimizes re-absorption affects such as the non-linear affects effect due to inner filter affects, which is when the emitted light is re-absorbed

before reaching the detector.[31] The absorbance of the two standards and the sample should be measured, and the absorbance should be plotted as a function of concentration. This Beer's Law plot indicates if the data does have a linear relationship which is needed in order to continue the analysis. The emission spectrum of each solution is then measured and a plot of integrated intensity of the emission maximum is plotted as a function of absorbance. This plot is used to determine the quantum yield itself by using Equation 1. In this experiment, the fluorescence quantum yield, which is the ratio of the number of photons emitted relative to the number absorbed by the molecule through fluorescence (as shown in Equation 1), was measured by utilizing both a UV-Vis spectrophotometer and a spectrofluorometer.

$$\phi_x = \phi_{st}\left(\frac{Grad_x}{Grad_{st}}\right)\left(\frac{\eta_x^2}{\eta_{st}^2}\right) \quad (1)$$

The ϕ is the quantum yield with ("x" relating to the experimentally determined quantum yield standard and "st" relating to the other standard which is acting as a reference), "Grad" is the slope of the integrated intensity versus absorbance plot, and η is the refractive index of the solvent used.

Once the emission is measured, the quantum yield of the osmium complex was determined using $[Ru(bpy)_3]^{2+}$ and $[Ru(phen)_3]^{2+}$ as standards. These standards were chosen due to the fact that both complexes have known and reasonable quantum yields obtained in water as well as similar excitation and emission spectra. These yields are 0.028 and 0.032 for $[Ru(bpy)_3]^{2+}$ and $[Ru(phen)_3]^{2+}$, respectively. It is hypothesized that the method developed by Horiba can be applied to determine the quantum yields of

compounds such as $[Os(CO)_2(sulf\text{-}dpp)Cl_2]$, which can then be incorporated into a MOF, eliminating the possibility of the leaching of the reporter molecule when the sensor is used in aqueous sensing.[31] It is important to note that for this work, rigidochromic behavior is not being characterized. Instead, the quantum yield measurements will determine whether or not incorporating the $[Os(CO)_2(sulf\text{-}dpp)Cl_2]$ into a MOF is logical based on sufficient anticipated response as indicated by the quantum yield.

Photophysical Characterization of Luminescent Compounds

In order to analyze any of the aforementioned reporter molecules, photophysical characterization must be performed. Photophysics is the study of how light energy, in the form of photons, interacts with matter. Unlike photochemistry, which is focused on how that interaction drives a chemical reaction, photophysics measures the absorption and emission of the light without the initiation of a chemical reaction.[32] These characteristics are measured quantitatively via spectrophotometry, either in the realm of UV-vis absorption spectrophotometry or luminescence spectrofluorometry. The absorption spectra of a molecule exhibit broad peaks known as absorption bands. These peaks correspond to very narrow ranges of wavelengths where the compound will absorb light. However, these transitions are more easily detected as emitted light, after the compounds have been excited and returned to their ground state configurations. The absorption peaks reflect the pattern of energy quantization in the atoms of the compound, and the wavelength of the peak can be used to determine the energy of the photons needed to

excite the electrons. Bohr postulated that light can only be absorbed if the energy of the photon matches the energy difference between two energy states within an atom. This line of reasoning can also be used for molecular compounds as well. Within Figure 9, it can be seen that varying amounts of energy in the form of light will excite the electrons in chlorophyll a into one of three excited states. All absorption peaks observed within this spectrum are due to the chlorin ring, which emits light much like that of a porphyrin ring. The absorption bands within these systems are actually due to mixing between the transition between two HOMOs and two LUMOs, resulting in two energy states: Soret bands which correspond to the higher energy state and lower excitation wavelength and Q-bands which correspond to the lower energy state and higher excitation wavelengths.[33]

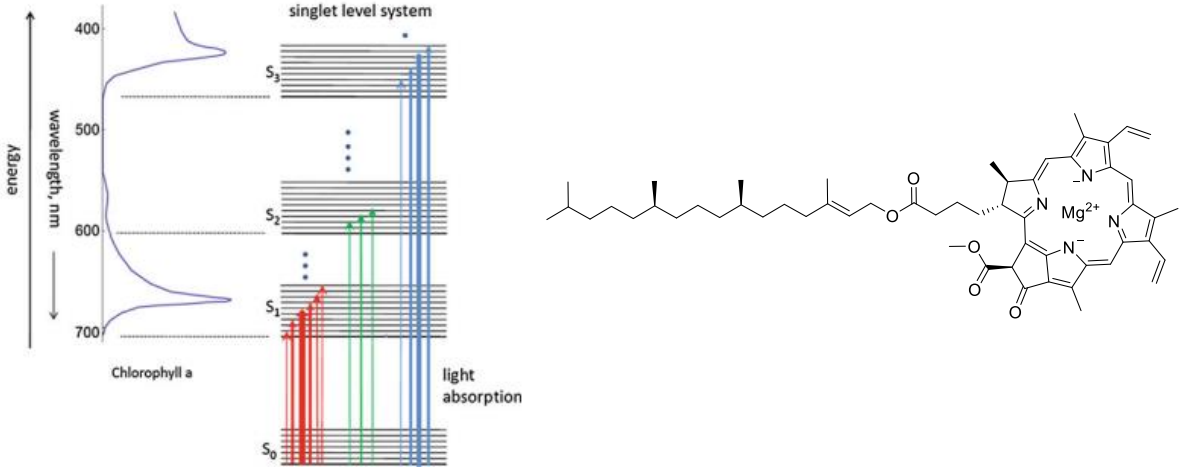

Figure 9: Molecular energy level scheme and its relation to the molecular absorption spectrum for chlorophyll a.[34]

Each excited state in a molecular compound is comprised of many more energy levels than atomic excited states, since, in atoms, energy can only be deposited as electronic excitation. Molecules have vibrational energy levels which are spaced

relatively uniformly with differences in energy much less than the electronic levels. This allows electrons to potentially excite into a higher vibrational state as opposed to just the electronic energy state, but these transitions typically are only seen in gas phase measurements. This is because in the solid and liquid phases electrons have more limited movement and there is a lower probability of their excitation into the vibrational energy levels of a given electronic state. Besides electronic and vibrational excitation, molecules can also rotate. This adds yet another set of energy levels with energy differences that are even smaller than the vibrational states.[35]

One thing that the absorption spectrum of a molecule shows is that the transition from the ground state to any of the electronic-vibrational-rotational states is not equally probable, since it is still the interaction of photons with the electrons that is responsible for the absorption of the electromagnetic energy. The probable transitions are called allowed transitions and are determined theoretically. However, the transitions in the useful region of the ultraviolet-visible spectrum range are usually $n \rightarrow \pi^*$ or $\pi \rightarrow \pi^*$, for organic compounds (where n is a non-bonding electron, π^* is an anti-bonding orbital, and π is a bonding orbital). TMCs can also experience metal to ligand charge transfers (MLCT) and ligand to metal charge transfers (LMCT). The probability, as determined through the use of quantum mechanics in conjunction with the amount of energy being introduced to the system, that the electrons will undergo any of these transitions within a given time in an electromagnetic field of a given wavelength and magnitude is what determines the intensity of the absorption band for the compound at a certain

concentration. This indicates which transitions are more favorable for the molecular system.

The excited states determined by the excitation and emission spectra can be described by photophysical processes as well. Every allowed excitation can be described by a Jablonski diagram (Figure 10). Within this scheme, there are two categories of excited states with one being a representation of the singlet, denoted with an S, and the other the triplet, denoted with a T, systems of the molecule. Of the two quantum states depicted, the singlet state is generally the ground state for a molecule given that the electrons in this state are paired and have a net nuclear spin of zero. This electron pairing also causes a singlet state to be the quantum state than is most likely occupied as the first excited state of the molecule since it has a more favorable quantum spin than a triplet state. The less favorable quantum spin the triplet states exhibit is due to the fact that these quantum states have three possible configurations comprised of unpaired electrons which results in a quantum spin number of one.

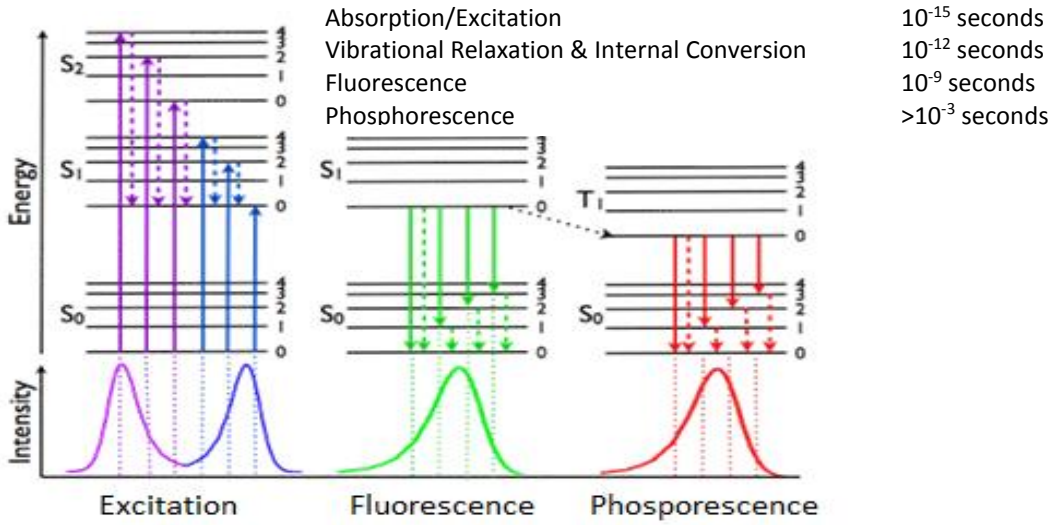

Figure 10: Jablonski diagram representing the typical photophysical properties in molecules with relative timeframe for each phenomena.[36]

Both the singlet and triplet higher energy quantum states (shown in Figure 10 as S_1, S_2, and T_1) can only be occupied if the molecule is excited. When a molecule is excited, at least two electrons will singly occupy molecular orbitals: one still in the ground state, the other excited to a higher energy state. Given that the triplet state is lower in energy than its singlet counterpart, it might be assumed that it would be more favorable for an excited electron to transition from the ground state to the lower energy of the two excited states. However, triplet states can only be populated via transitions from a higher energy singlet state and usually requires an overlap of the vibrational states of the higher singlet state and the triplet state (shown in Figure 10) known as intersystem crossing. This is due to the fact that the transition from the ground singlet state to the excited triplet state is more improbable than the singlet to singlet transition usually observed; the difference between the electronic states of the S_0 and T_1 states requires a great deal of energy in order of the transition to occur. Thus, the state an excited electron will populate is initially actually a singlet state.

After a molecule is excited into a higher vibronic, i.e. vibrational and electronic excited state, radiationless transitions (shown as the dotted lines in Figure 10) can occur. These transitions include vibrational relaxation and internal conversion. Vibrational relaxation can happen when one vibrating molecule collides with its surroundings, which transfers the energy in the form of heat and results in relaxation of the molecule to a lower energy vibrational state. Internal conversion occurs when an electron in a higher vibrational level of either the S_1 or S_2 state is relaxed down to a different lower excited state with the same multiplicity. Emission from a singlet excited state is known as

fluorescence and is readily exhibited by luminescent organic dyes.[5] There is also the possibility that the excited electrons could experience intersystem crossing— a process which can only happen when there is a magnetic field applied because a spin flip is required of the unpaired electron. When the molecule begins to relax from the triplet excited state, if it possesses the correct properties, a spontaneous, undirected emission specific to the molecule occurs. This phenomenon is known as phosphorescence. Unlike fluorescence, phosphorescence is not a luminescence characteristic demonstrated by the majority of luminescent organic molecules. In order for a molecule to phosphoresce, the presence of a heavy atom helps to facilitate the required intersystem crossing, which then enhances the luminescent quantum yield.[5] This is due to a phenomenon known as the heavy atom effect that is simply the enhancement of rate of a spin-forbidden process by the presence of a heavy atom within a system due to the response the process has to the spin-orbit coupling enhancement produced by the atom.[37]

As indicated, absorption, excitation, and emission spectra as obtained for the compounds reported here are analytical measurements that provide vital information regarding a compound's luminescent properties, collected from the Stokes shift and vibrational structure, and thus its ability to act as part of a luminescence-based sensor.[32,35] Within this body of work, both the singlet and triplet excited states are of interest. Organic dyes such as DSA mainly exhibit fluorescence while TMCs like the type investigated here will exhibit a combination of fluorescence and phosphorescence.

Experimental

The reagents for this work were used as received and are as follows: $(NH_4)_2OsCl_2$ (99.99%, Alfa Aesar), formic acid (90%, Fisher Scientific), formaldehyde (37%, Acros), dichloromethane (99.8%, Acros), $[Ru(bpy)_3]Cl_2$ (GFS Chemicals), $[Ru(phen)_3]Cl_2$ (GFS Chemicals), hexane (99.9%, Fisher Scientific), chloroform (99.9%, Fisher Scientific), acetone (99.8%, Fisher Scientific), acetonitrile (99.9%, Fisher Scientific), methanol (99.8%, Acros), DMSO (99%, Aldrich), benzene (99.9%, Fisher Scientific), acrylamide (99%, Acros), 2-(dimethylamino)ethyl methacrylate (DMAEM, 99%, Acros), *N*,*N*'-methylenebisacrylamide (BIS, 96%, Acros), Nitrogen gas (99.5%, Roberts Oxygen Company), Drierite desiccant (8 mesh, Acros), LiBr (99%, Acros), LiCl (Certified ACS, Fisher Scientific), KCH_3CO_2 (Certified ACS, Fisher Scientific), $MgCl_2$ (Certified ACS, Fisher Scientific), $Mg(NO_3)_2 \cdot 6H_2O$ (98%, Acros), NaBr (Certified ACS, Fisher Scientific), NaCl (Certified ACS, Fisher Scientific), KCl (Certified ACS, Fisher Scientific), K_2SO_4 (Certified ACS, Fisher Scientific), potassium persulfate (99%, Sigma Aldrich), DSA (Invitrogen), $[Os(CO)_2(sulf\text{-}dpp)Cl_2]$ (prepared by Amy Wagner, 2012), and compound **1** (prepared by Chris Ryan, 2014). Standard safety precautions were followed and all waste was collected and disposed of in accordance with the Safety regulations of the Elizabethtown College Department of Chemistry and Biochemistry.

Fluorescent Organic Dye

Solvent Study: DSA and Derivatives

The effect of different solvents on the fluorescence characteristics of DSA was determined by modifying a method used by Diwu *et al.*[30] The solvents studied were: hexane, chloroform, acetone, acetonitrile, methanol, DMSO, and DI water. For each solvent, a small amount (less than 1 mg) of the DSA dye was dissolved, and the solution was diluted until the absorbance was below 0.1. The absorbance was measured using the Shizmadzu Model UV-2401PC UV-Visible Spectrophotometer. The maximum absorbance wavelength was recorded for the compound in each solvent and used as the excitation wavelength for the emission measurements. Both emission and excitation spectra were obtained on the Horiba Jobin Yvon Fluorolog-3 Model FL3-22 Spectrofluorometer with the slit width set to 1 nm. The maximum emission wavelength for each solvent was used for the excitation measurement. The data collected for each set of measurements included the maximum absorbance wavelength and absorbance of each peak, the maximum emission wavelength, and the maximum excitation wavelength. The resulting spectra were then normalized to a maximum intensity of 1.

This same procedure was used to analyze the solvent effect on the fluorescence characteristics of **1**. The solvents studied were the same except that benzene was substituted for hexane since **1** was not soluble in hexane, and minute quantities of methanol and chloroform were added to water also due to solubility issues, creating a solution of 8% methanol, 5% chloroform, and 87% water. Gravity filtration was used in

order to remove particles of the dye that had not dissolved in order to prevent detection of scattered radiation upon acquisition of spectral data.

Polymerization of hydrogel

Compound **1** was polymerized into a smart hydrogel following the procedure used by Tellis *et al.*, but with **1** in replace of the commercially available DSA.[27] The nitrile DSA derivative (0.0005 wt %) was added to a solution comprised of acrylamide (57 wt %), DMAEM (40 wt %), and BIS cross-linker (3 wt %) to give a concentration of 50 μM. The solution was stirred for 20 min under inert atmosphere. After the allotted time, potassium persulfate initiator (0.2 wt %) was added. After 1 min of continued stirring, 400 μL of the monomer solution was placed onto a prescored glass microscope slide (7.6 cm x 2.5 cm x 1 mm) via microliter pipet; the slide was scored with a glass scorer into quarters with dimensions of 3 cm x 0.8 cm in order to all each gel to be placed within a sample cuvette. The solution was evenly distributed on the face of the slide and then allowed to polymerize and dry for 4 days at room temperature. Once dried, the slide was placed into a laboratory oven set at 60 °C for 2 h.

Calibrations of the gels were performed in still air. This was accomplished by preparing saturated salt solutions of desired relative humidity (RH): 0% RH, Drierite; 6% RH, LiBr; 11% RH, LiCl; 21% RH, KCH_3CO_2; 33% RH, $MgCl_2$; 54% RH, $Mg(NO_3)_2 \cdot 6 H_2O$; 57% RH, NaBr; 75% RH, NaCl; 85% RH, KCl; 98% RH, K_2SO_4.[38] Each solution was allowed to equilibrate in a closed container at room temperature, and then the gel

was introduced, in a quartz cuvette, into the environment for 75 min. The cuvette was then capped and the emission of the sensor was measured with excitation wavelengths of 323 nm, 340 nm, and 356 nm; each maximum emission wavelength was recorded. All measurements were performed in front-face mode, with the sample oriented so that it was facing the source and detector, instead of the usual right angle orientation with a triangular cuvette, in order to reduce scattering. The resulting spectra were then normalized to a maximum of 1. The gel was also tested for leaching to ensure that **1** did polymerize into the hydrogel and was not just embedded. This was accomplished by washing the gel numerous times and measuring the intensity of the emission maximum after each subsequent wash.

Luminescent Transition Metal Complex

Synthesis of $[Os(CO)_2(sulf\text{-}dpp)Cl_2]$

The synthesis of $[Os(CO)_2Cl_2]$ was performed following the procedure of van Slageren *et al.*[17] All reactions were performed under inert atmospheric conditions using a Schlenk line. A 100 mL Schlenk flask was evacuated and then flooded with N_2 gas. To this flask, 420 mg (0.95 mmol) $(NH_4)_2OsCl_2$, 40 mL (0.87 mmol) formic acid, and 15 mL (0.50 mmol) formaldehyde were added. The resulting solution was a deep red-brown color. Nitrogen gas was allowed to bubble through the system for 30 min, after which the color of the solution changed to amber. The solution was refluxed at 102 ºC for 3 days. After 24 h, the solution was dark yellow-green which progressed to yellow at the end of

the reflux period. The solvent was removed via roto-evaporation, leaving a dark brown-yellow oil. The oil was stored at 4 ºC, forming a green-brown solid. This solid was triturated with 20 mL of dichloromethane for 1 h. During this time, the solvent turned a light yellow color. The solution was filtered, 15 mL of acetone was then added to the dichloromethane filtrate, and the solvents were allowed to evaporate. Gentle heating was used to help facilitate the evaporation. This resulted in the formation of dark amber crystals. ATR-FTIR analysis, performed on the Nicolet iS10 Fourier-Transform Infrared Spectrometer, was used to characterize the synthesized compound. To increase purity, the product was recrystallized in acetone, resulting in larger dark amber crystals, and IR analysis was again performed. The reaction was repeated two more times; the most distinctive differences were total reaction times. One of the reactions was allowed to progress for 3 days, resulting in a 40% yield, while the other only 2 days, resulting in yields of 18% and 16%.

The synthesis of the $[Os(CO)_2(sulf\text{-}dpp)Cl_2]$ was modified from a published procedure.[17] This complex was synthesized by refluxing 115.9 mg (0.22 mmol) bathophenanthrolinedisulfonic acid disodium salt hydrate and 46.2 mg (0.15 mmol) $[Os(CO)_2Cl_2]$ in a 3:2 mole ratio for 8 h at 90 °C in 15 mL of 2-propanol with 2 mL of water to increase the solubility. Periodically, the reaction was tested to ensure conversion of the $[Os(CO)_2Cl_2]$ to $[Os(CO)_2(sulf\text{-}dpp)Cl_2]$ by performing IR analysis and monitoring the decrease in the signals at 2122 cm^{-1} and 2012 cm^{-1} (which correspond to the $[Os(CO)_2Cl_2]$) and the increase in the signals at 2136 cm^{-1}, 2037 cm^{-1}, and 1960 cm^{-1} (which correspond to the $[Os(CO)_2(sulf\text{-}dpp)Cl_2]$). Once the reaction was complete, the

solvent was removed via vacuum and gentle heating. The crude yield of this reaction was 237%, indicating that further purification is required.

Quantum Yield Measurements: $[Ru(bpy)_3]Cl_2$ and $[Ru(phen)_3]Cl_2$ Standards and $[Os(CO)_2(sulf\text{-}dpp)Cl_2]$

The fluorescence quantum yields of $[Ru(bpy)_3]Cl_2$, $[Ru(phen)_3]Cl_2$, and $[Os(CO)_2(sulf\text{-}dpp)Cl_2]$ were measured using the procedure described by Horiba.[31] As mentioned previously, this method used a series of solutions of varying concentration in order to obtain absorbance values of approximately 0.1, 0.08, 0.06, 0.04, 0.02, and 0. A 2.00×10^{-5} M $[Ru(bpy)_3]Cl_2$ solution, and a 2.10×10^{-5} M $[Ru(phen)_3]Cl_2$ solution were prepared as well as a 4.95×10^{-5} M $[Os(CO)_2(sulf\text{-}dpp)Cl_2]$ solution. From these stock solutions, all other standards were prepared. The concentrations of standard solutions (all in M) are: 6.80×10^{-6}, 5.60×10^{-6}, 4.00×10^{-6}, 2.80×10^{-6}, and 1.20×10^{-6} for $[Ru(bpy)_3]Cl_2$; 8.40×10^{-6}, 7.06×10^{-6}, 5.88×10^{-6}, 4.20×10^{-6}, 2.52×10^{-6} for $[Ru(phen)_3]Cl_2$; and 3.87×10^{-8}, 7.73×10^{-8}, 1.16×10^{-6}, 1.55×10^{-6}, 2.06×10^{-6} for $[Os(CO)_2(sulf\text{-}dpp)Cl_2]$. The absorbance of each solution was measured using the Shizamdzu Model UV-2401PC UV-Visible Spectrophotometer, which was set to the parameters listed in Table 1. The maximum wavelengths and absorbance of each peak were recorded for each standard using 1 cm matched quartz cuvettes. The results were then plotted in a Beer's Law plot using Equation 2:

$$A = \varepsilon bc \quad (2)$$

where A is the absorbance of the standard solution, ε is the molar extinction coefficient ($L \cdot mol^{-1}cm^{-1}$), b is the path length (cm) the source light travels through the sample, and c is the concentration of the standard solution (M).

Table 1: Parameters for absorbance measurements of $Ru(bpy)_3]Cl_2$ standards, $[Ru(phen)_3]Cl_2$ standards, and $[Os(CO)_2(sulf\text{-}dpp)Cl_2]$ standards.

Measurement Parameters	
Wavelength range	700-300 nm
Scan Speed	Medium
Sampling Interval	1.0 nm
Scan Mode	Normal
Light Source Change Wavelength	297 nm
Slit Width	5 nm

The emission spectrum of each solution was also measured as well as the excitation spectrum of the standard of highest concentration. These measurements were performed on the Horiba Jobin Yvon Fluorolog-3 Model FL3-22 Spectrofluorometer, set to the parameters specific to each complex with the only consistency being that the slit widths were set to 5 nm and the beam was at a right angle. The $[Ru(bpy)_3]Cl_2$ standard was excited at 454 nm and had a scan range of 465-800 nm for the emission measurements, while the excitation measurements had an emission wavelength of 605 nm and a scan range of 200-590 nm. The excitation wavelength used for the $[Ru(phen)_3]Cl_2$ standard was 447 nm, and the range was 457-800 nm. A wavelength of 592 nm and a scan range of 200-570 nm was used for the excitation measurements. For $[Os(CO)_2(sulf\text{-}dpp)Cl_2]$, emission measurement had an excitation wavelength of 500 nm and a scan

range of 510-800 nm, while the excitation measurement had an emission wavelength of 700 nm and a scan range of 710-850 nm.

The excitation wavelengths used for emission measurements were determined using the peak corresponding to the MLCT transitions in the absorption spectra, while the emission wavelengths used for the excitation measurements was found by using the most intense peak in the emission spectra. The emission and excitation measurements were performed with polarizing filters in order to reduce scattering and the detection of source radiation, but also without filters in case signals with filters were insufficient for accurate measurement. The polarizing filters were oriented 90° relative to each other (with the emission filter set to 90° and the excitation set to 0°) and placed after the source and before the detector. For all measurements, the maximum excitation and emission wavelength, intensity at that wavelength, and integrated intensity of each peak were recorded for each standard.

Results & Discussion

Fluorescent Organic Dye

Solvent Study: DSA and Derivatives

In order to provide a basis to which all future measurements are compared, absorption, excitation, and emission measurements were performed for the DSA dye. It is expected, based on the stabilization of the excited state of DSA, that more polar solvents

would result in a slight increase in the absorption wavelength as well as in the excitation wavelength. The emission wavelengths should also increase with an increase in solvent polarity since the excited state of the DSA is more stable in more polar solvents due to TICT. This hypothesis was tested by dissolving DSA in solvents of varying polarity and collecting the corresponding absorption, excitation, and emission spectra.

The absorption spectra of DSA dissolved in various solvents are shown in Figure 11. A general trend that should be noted is that as the solvents increase in polarity, the maximum absorption wavelength shows a small increase, as expected. However, the overall order of increasing wavelength in accordance with the polarity of the solvent varies slightly from what would be expected based on stabilization of the excitation state of DSA by more polar solvents. The predicted order of the solvents would be based slightly on the polarity of each (Table 2) with the less polar having a maximum absorption at a shorter wavelength and the most polar absorbing at a longer wavelength: hexane would be first while water would be last. This is due to the fact that, in polar solvents, the $\pi \rightarrow \pi^*$ transitions are more pronounced since the excited state is more stabilized, lowering the energy of the transition and resulting in an observed red-shift in the absorption maximum. The $n \rightarrow \pi^*$ transitions were predicted to be less relevant, in comparison, because this transition will result in a blue-shift with increase in solvent polarity.

Table 2: $E_T(30)$ empirical solvent polarity parameters of the solvents used.

Solvent	Polarity
Hexane	31.0
Benzene	34.3
Chloroform	39.1
Acetone	42.2
DMSO	45.1
Acetonitrile	45.6
Methanol	55.4
Water	63.1

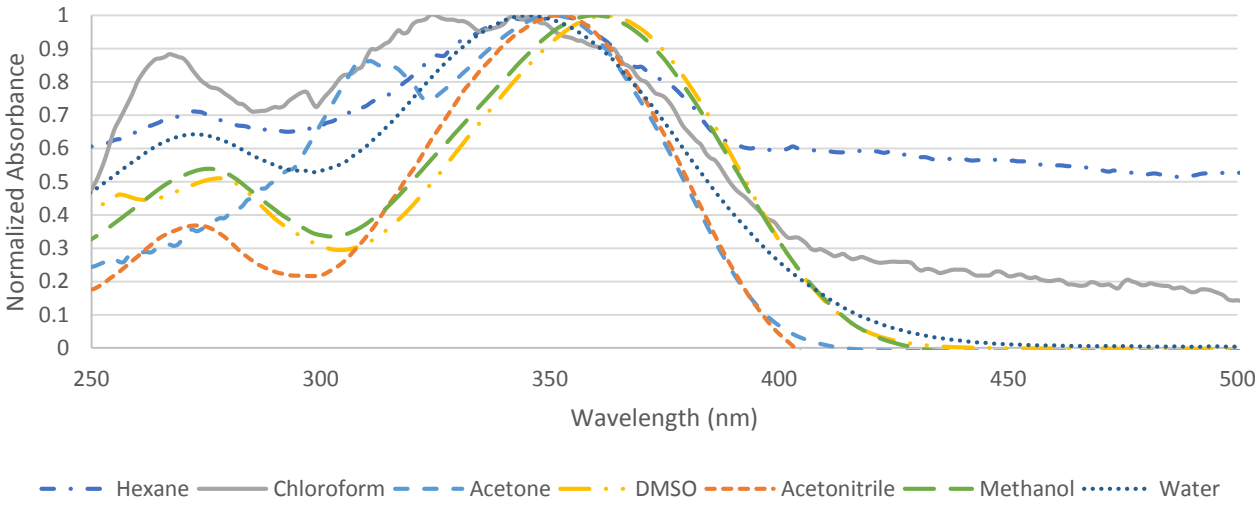

Figure 11: Normalized absorbance spectra for DSA in solvents of varying polarity as a function of wavelength.

The experimental results did not completely follow the expected trend in that chloroform was absorbing at the smallest wavelength, water was absorbing around the same wavelength as chloroform, and DMSO was absorbing at the second highest. The observed insensitivity suggests that the interaction between solvent and participative ground and excited states of the molecule is such that the energy gap between the ground

state and excited states responsible for the observed transitions is independent of the polarity and hydrogen-bonding of the solvent.[11]

The excitation spectra of DSA dissolved in various solvents are shown in Figure 12 when collected at an emission wavelength ranging from 400 nm to 575 nm. For this collection of spectra, all of the maximum wavelengths are within the 350 nm to 375 nm range, except for DMSO which peaks at 426 nm. The lack of peaks at lower wavelengths, which were present in the absorption spectra indicates that the emission at the optimum excitation wavelength does not originate from the higher energy excited state, which indicates that internal conversion is not occurring.

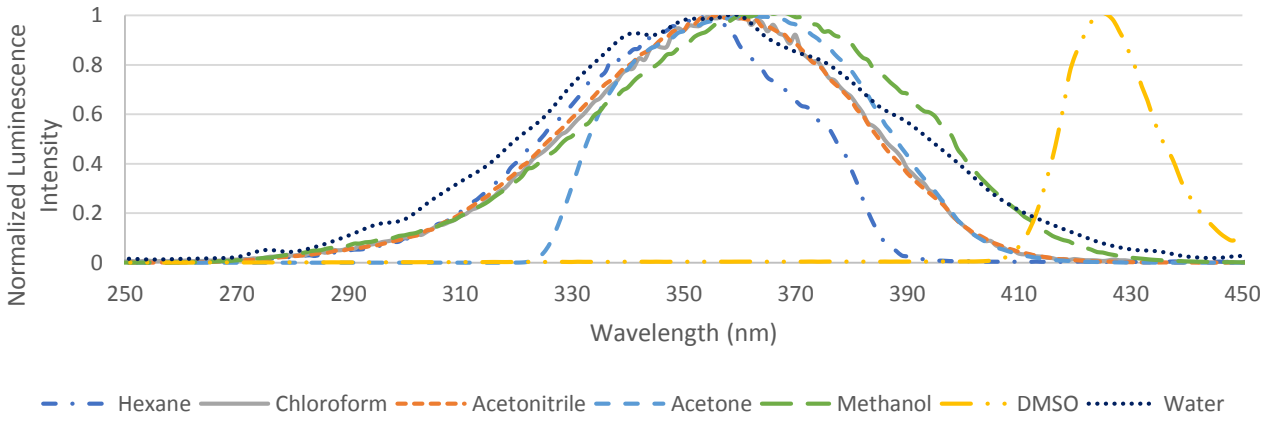

Figure 12: Normalized excitation spectra for DSA in solvents of varying polarity as a function of wavelength.

It is interesting to note that the excitation spectra do not resemble the absorption spectra very strongly for all of the solvents; the peaks of the excitation spectra are better defined than the absorption spectra peaks and the ordering of the solvents from shortest to longest maximum excitation wavelength follows what was predicted more closely.

However, DMSO is still not following the trend since this solvent resulted in the longest excitation wavelength, not water as was predicted.

The excitation data collected for the dye also failed to follow the predicted trend in that the DMSO spectrum peaked at the highest wavelength of all the solvents tested. This then also suggests that the excitation wavelength of the DSA dye is fairly insensitive to the polarity and hydrogen bonding ability of each solvent. This is not an unreasonable conclusion since excitation and absorbance properties are directly related to one another and so share similar properties. The maximum excitation peak was used in the Stokes shift calculations for each solvent.

The emission spectra of DSA dissolved in various solvents are shown in Figure 13. Overall, the spectra exhibit the same trend as the absorption and excitation spectra and show an increased red-shift with an increase in solvent polarity. There is one anomaly in the spectral shape; when DSA was dissolved in hexane, a more resolved structure of the single peak was observed instead of the broad band seen with the other solvents; this is due to the inability of hexane to stabilize the excited state of DSA which results in the ability to visualize the vibrational modes of the molecule. The order of shortest wavelength to longest for this set of spectra again deviates from the predicted based on the expected effect of the solvent environment. This is showing hexane with the shortest maximum wavelength, which was expected, but acetone and chloroform changed positions in the list. Water, methanol, DMSO, and acetonitrile are still the solvents that yield the longest maximum emission wavelengths. One observation of interest is the

presence of a second excited state when DSA is dissolved in water as indicated by the second peak at 412 nm.

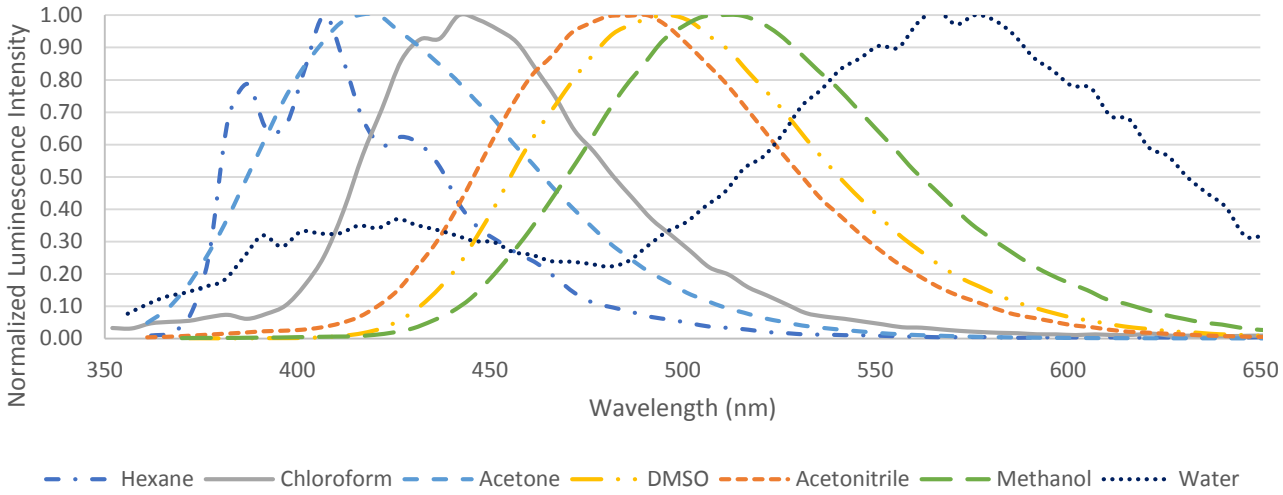

Figure 13: Compilation of normalized emission spectra for DSA in solvents of varying polarity as a function of wavelength.

Compared to the absorption and excitation spectra, the emission spectra of the solvents fit the predicted trend best. This suggests that the emission wavelength of the dye is solvent-sensitive, which was expected since an increase in polarity of the environment would stabilize the excited state of the molecule and lower the energy difference between the excited and ground states.

The Stokes shift of DSA plotted against each of the different solvents is displayed in Figure 14. Overall, the data were fairly linear and resulted in an R^2 value of 0.7154, indicating a correlation between polarity of the solvent and Stokes shift. Both DMSO and acetonitrile deviate fairly significantly from the trend, this could be due to the two excited states competing with neither being more favorable in solvents of moderate polarity. The

general trend that can be seen from this plot is that, as polarity of the solvent environment increases, so too does the Stokes shift.

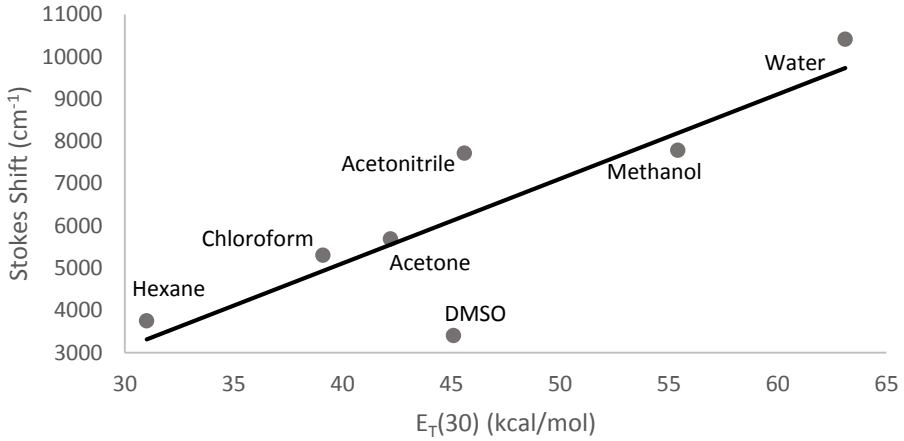

Figure 14: Plot of Stokes shift of DSA vs solvent polarity parameter $E_T(30)$.

From the data collected, it can be concluded that the fluorescence properties of DSA are dependent on the polarity of solvent environment. The Stokes shift of the dye was measured in solvents with $E_T(30)$ polarity values ranging from 30 to 65 and were plotted as a function of the solvent polarities. The resulting trend was linear, which was consistent with Diwu's results.[11] Unlike Diwu's experiment, it was not found that the fit increased with the exclusion of the methanol data. Rather, it would improve with the exclusion of either the DMSO or acetonitrile data. This can still imply that there are not only dipole-dipole interactions affecting the energy levels of the excited dye, but also hydrogen bonding interactions. This difference in data may be due to the fact that, unlike Diwu, methanol was not the most polar solvent tested. The solvent effect of water was also measured, eliminating the deviation of methanol from the trend line. This indicates that the solvent sensitivity of the DSA dye is good enough to be a reliable comparison to

measurement of DSA derivative in order to determine the general solvent dependence of the fluorescence properties of compound **1**.

In order to determine the Stokes shift of compound **1**, measurements similar to the ones performed for DSA were conducted. It was predicted that the absorption and excitation measurements would not be very solvent-sensitive while the emission measurements would, based on the results of the DSA measurements. This hypothesis was tested by also dissolving compound **1** in solvents of varying polarity (generally the same as those used for DSA) and collecting the corresponding absorption, excitation, and emission spectra.

The absorption spectra of compound **1** dissolved in various solvents are shown in Figure 15. A general trend that should be noted is that solvent polarity did not appear to affect the maximum wavelength absorbed, unlike the trend observed when the absorbance of DSA was measured in the solvents. One anomaly that occurred was when the derivative was dissolved in acetone; there was a sudden oscillation of the absorbance of compound **1** at wavelengths 325 nm and lower. This oscillation was not observed in the excitation spectrum, as might be expected.

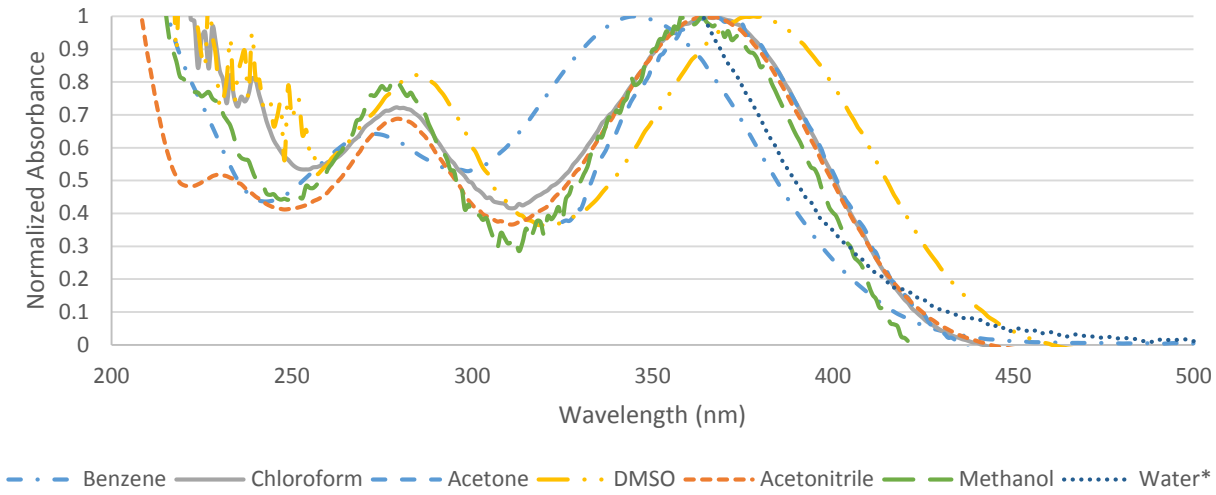

Figure 15: Normalized absorbance spectra for compound **1** in solvents of varying polarity as a function of wavelength. *87% water, 8% MeOH, 5% chloroform

The excitation spectra of compound **1** dissolved in various solvents are shown in Figure 16. For this collection of spectra, all of the maximum wavelengths are approximately 365 nm with the DMSO peak falling around 385 nm. Most peaks are similar in shape with both the acetone and DMSO peaks varying. The acetone peak flat-lines until approximately 325 nm and then sharply increases in intensity until it conforms to the shape of the other peaks. This is in direct contrast to what was observed for the absorbance peak. The DMSO peak is not as uniform as the other peaks present given that there appears to be a mini peak "budding" from the main peak. This is possibly due to an overlap of two different excited states as seen with DSA. The location of the water peak is also most likely due to the presence of a second excited state.

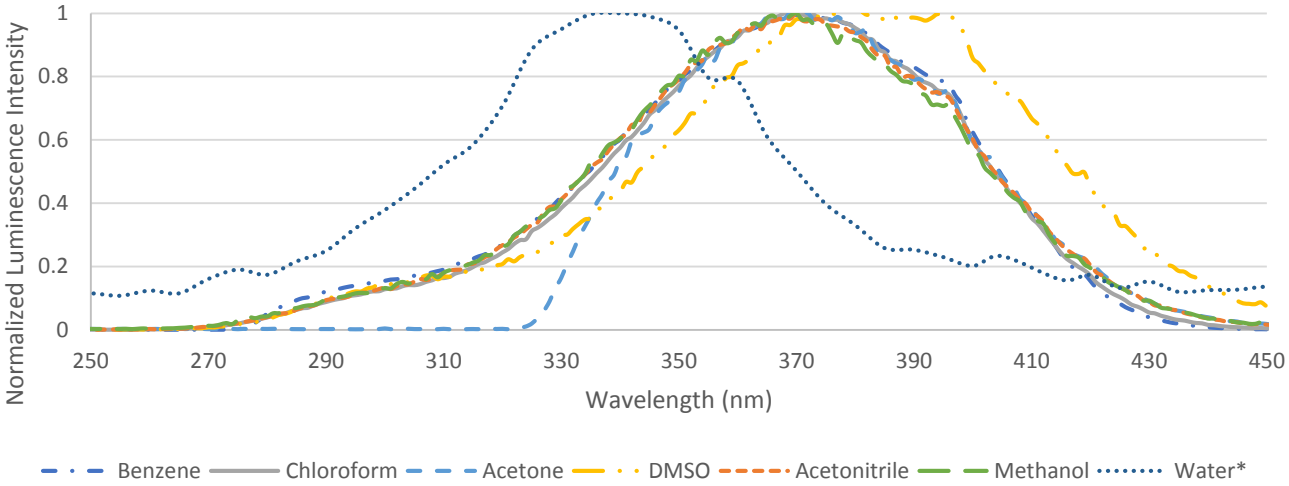

Figure 16: Normalized excitation spectra for the compound **1** in solvents of varying polarity as a function of wavelength. *87% water, 8% MeOH, 5% chloroform

The emission spectra of compound **1** dissolved in various solvents are shown in Figure 17. The separation of the peaks is rather good, which allows for a clearer analysis of the data. Overall, the spectra exhibit the same trend and show an increase in the red-shifting of the maximum wavelength with an increase in solvent polarity. When dissolved in chloroform, the maximum emission wavelength produced was the shortest, as expected based on the DSA data. It was interesting that the DMSO environment produced the longest maximum wavelength followed by methanol and acetonitrile which both had nearly identical maxima. The overall order from shortest maximum emission wavelength to longest was: chloroform, acetone, acetonitrile, methanol, and DMSO. The low maximum emission wavelength of the water peak also does not follow the original prediction given that water should stabilize the excited state of compound **1** the most, thus lowering the energy between the lowest excited state and the ground. This anomaly is most likely caused by the presence of a second excited state; the lower wavelength

indicates that the excited state from which the electrons are relaxing from is higher in energy and thus, must not be the TICT state.

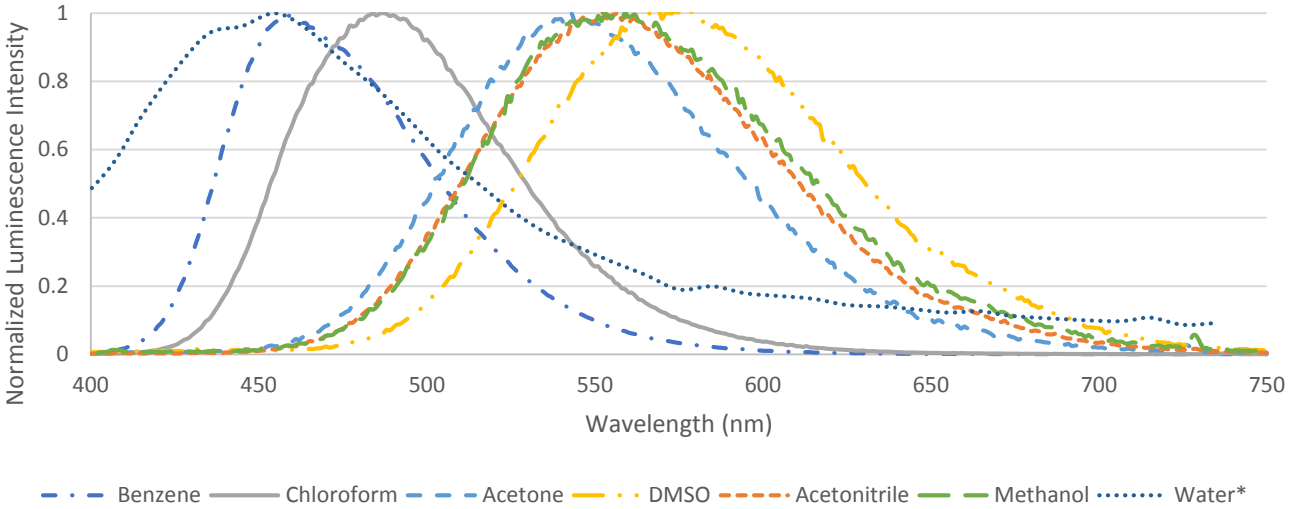

Figure 17: Normalized emission spectra for compound **1** in solvents of varying polarity as a function of wavelength. *87% water, 8% MeOH, 5% chloroform

The Stokes shift of compound **1** plotted against each of the different solvents is displayed in Figure 18. Within this figure are the data from both DSA and the Diwu derivative analysis. Overall, the data is relatively linear with R^2 values for the DSA data (0.715) and Diwu data (0.871) all ranging close to 1 with the exception of the compound **1** data (0.408), which was not very linear. If the Stokes shift of the DSA derivative in water is treated as an outlier and removed from the analysis, the R^2 value improves to 0.800. The slopes of the data sets, which are within experimental error of one another, are as follows: DSA 200 ± 56, Diwu derivative 201 ± 24, and compound **1** 195 ± 43 (slope of the line before the plateau). The general trend seen from this plot is that as polarity of the solvent environment increases, so too does the Stokes shift.

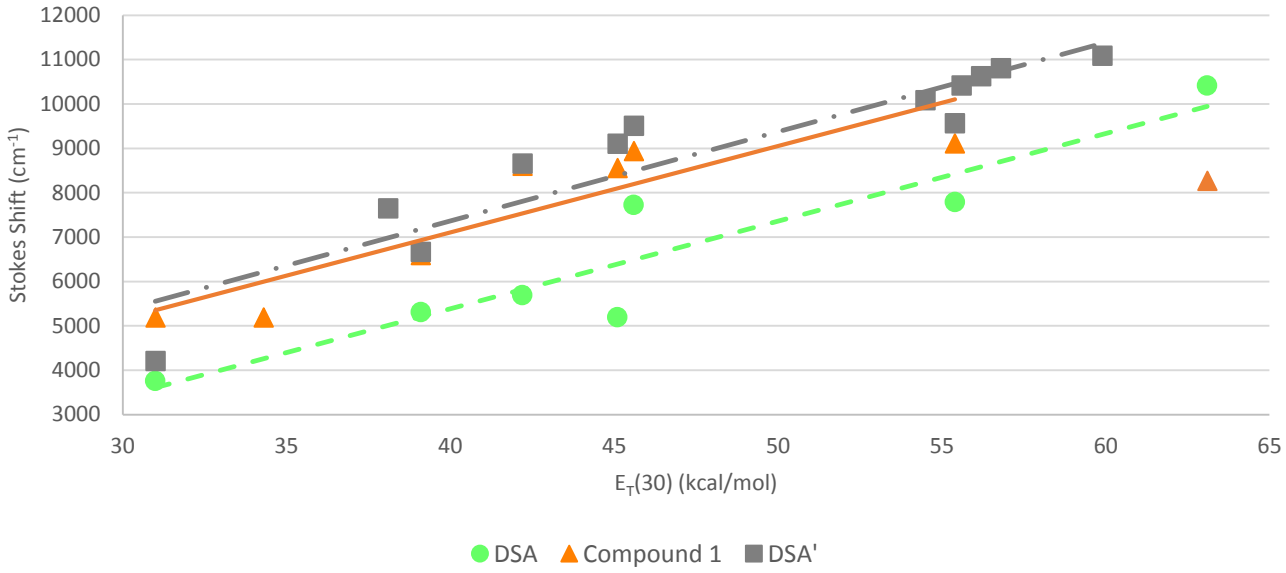

Figure 18: Lippert Plot of Stokes shift of Compound* vs solvent polarity parameter $E_T(30)^+$. *DSA, compound **1**, and Diwu derivative. +Hexane (31.0), Benzene (34.3), Chloroform (39.1), Acetone (42.2), DMSO (45.1), Acetonitrile (45.6), Methanol (55.4), and Water (63.1).

It is interesting to note that there may be a limit to the solvent sensitivity of compound **1**; there is no apparent change in Stokes shift after the molecule is exposed to a solvent with a polarity greater than 45. However, this may be because the Stokes shift is calculated relative to a different excitation peak. The plateau thus seems to suggest where the second excited state starts to compete with the TICT state. In most cases, these two are close enough in energy that only one peak is seen from the TICT. However, when **1** is within a more polar environment, the TICT state becomes distinct (Figure 19). It is possible that S_1^* can only occur in solvents with much higher polarity and/or extensive hydrogen-bonding.

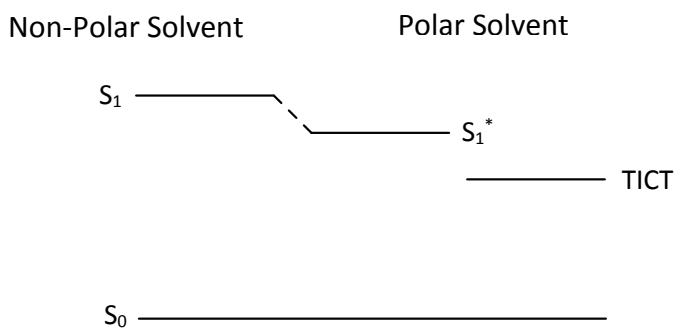

Figure 19: Suggested general solvent effect on the excited state of compound **1**.

Overall, the data depicted in Figure 18 suggest that compound **1** is solvent sensitive with similar sensitivity as DSA and the derivative synthesized by Diwu *et al.* However, the linear response in the sensitivity of compound **1** starts to break down once exposed to a highly polar environment. This may be due to the presence of two excited states, the known lower TICT state and a higher energy singlet excited state that experiences stabilization only through general solvent effects. The presence of this additional state prompted the identification of the optimum excitation wavelengths for each of the two excited states. These measurements led to the identification of 323 nm being the ideal wavelength for the higher energy excited state and 356 nm being the ideal wavelength for the TICT state. In future work, the Lippert plot should be obtained using each excitation wavelength. In the current work, all Stokes shifts were calculated relative to the lower energy excited state which had an excitation maximum at 340 nm. If the second excited state is taken into account, the Stokes shift for **1** in water might increase to 200 nm instead of the reported 95 nm shift.

Polymerization of hydrogel

Given that compound **1** exhibited some solvent sensitivity, the compound was polymerized into a smart hydrogel. This method of introducing the reporter molecule was performed in order to limit the potential of the leaching of the dye once moving on to aqueous phase measurements and to determine what effect, if any, the covalent attachment could have on solvent sensitivity. The excitation wavelengths used for these measurements were 323 nm and 356 nm, since these wavelengths were found to be the optimal excitation wavelengths for the two excited states of DSA, as well as 340 nm since this wavelength was found to be the optimal excitation wavelength for compound **1**. It was predicted that compound **1** could respond one of two ways. The fluorophore, which will experience a largely hydrophobic environment when covalently bonded, might be more sensitive to subtle differences upon influx of the polar solvent. Alternatively, the sensitivity of the fluorophore might decrease, because the ability of the dye to perform a TICT may be hindered due to the covalent bond. Neither of these relate to results of the previous smart hydrogel polymerized since the DSA was not incorporated into the gel itself and so, was continuously exposed to a predominantly polar environment.

The results of the characterization of the smart hydrogel are quite interesting (Figure 20). When excited at 323 nm (A), the presence of the higher energy excited states can be seen, but there is a hump present to the right of the maximum, which was not expected, thus broadening the peak indicating that the two excited states are in competition with one another.

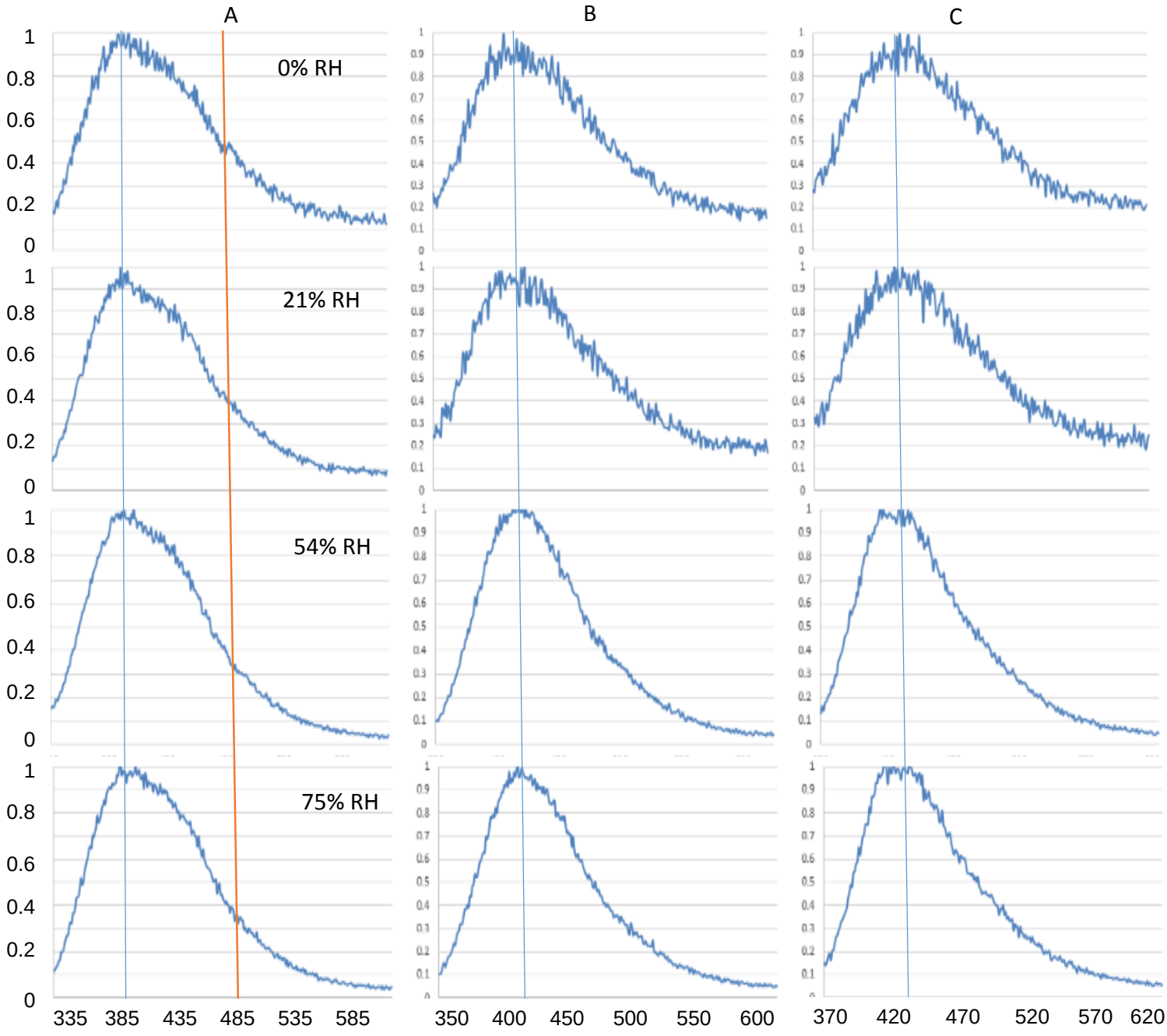

Figure 20: Emission spectra for smart hydrogel polymerized with compound **1** in varying levels of relative humidity excited at: 323 nm (A), 340 nm (B), and 356 (C).

Since the excitation wavelength used was the optimal wavelength for the higher energy excited state, it was predicted that only this state would be present in the resulting spectra. The prominent maximum, which is indicative of the higher energy excited state, is consistently observed at 400 nm. With an increase in the relative humidity, the peak begins to narrow with an increase in favoring of the higher energy excited state. The decrease in broadening of the peak with increase in analyte (i.e., water) concentration follows the trend of increased population of the S_1^* state with an increase in environment polarity. This indicates that the excited state is less stabilized with higher analyte concentration, supporting the second hypothesis since an increase in concentration of water might hinder the ability of the dye to perform a TICT.

When the gel was excited at 340 nm (B), it can be seen that there is no shift in the maximum emission wavelength with increased relative humidity. Since this wavelength was between the two optimum wavelengths for the two respective excited states, it was predicted that both might be visible. Instead, the two were apparently averaged, resulting in a single peak at 420 nm. The lack of response to a change in analyte concentration indicates, again that incorporating the fluorophore directly into the smart hydrogel might have hindered its ability to perform a TICT, which would result in virtually no stabilization of the associated excited state. It could also be possible that a stabilization is occurring, but only at higher analyte concentration as indicated with the sudden presence of a hump around 440 nm, which is indicative of emission from the lowest excited state.

The data collected when the excitation wavelength was 356 nm demonstrates another trend. This set of spectra were predicted to only show the peak corresponding to

the lowest energy excited state since this was found to be the optimal excitation wavelength for that state. This prediction holds true for the range of relative humidities tested. This again, indicates that the polymerization of the fluorophore into the hydrogel hinders the ability of the molecule to enter the TICT state.

The results of the humidity calibration were not consistent from one excitation wavelength to the next and are complicated by the apparent population of two different excited states. Exciting at shorter wavelengths should result in only observing the higher excited state, but in actuality resulted in the most dynamic results; there was a demonstration of solvent sensitivity by the gel, albeit slight. The longer excitation wavelengths resulted in little to no sensitivity of the solvent, however, the sensitivity that was shown supports results from the data collected with an excitation wavelength of 323 nm. Overall, it appears that compound **1** can be used in a humidity sensor, but the analysis must be performed using shorter excitation wavelengths and will only be reliable to a certain extent since the TICT state started to destabilize with an increase in relative humidity. In future work, it would be ideal to investigate the ratios of intensities obtained at each peak to determine whether they exhibit a dependence on relative humidity.

If compound **1** were leaching from the hydrogel, a similar plot as seen in Figure 21 was expected. However, the leaching tests revealed that compound **1** did polymerize into the hydrogel given the relative consistent intensity of the first four washes and the last four, as shown in Figure 22. The slight increase and decrease seen in the middle three washes could be due to a structural change experienced by the hydrogel or it could be caused by an orientation change during the emission measurements.

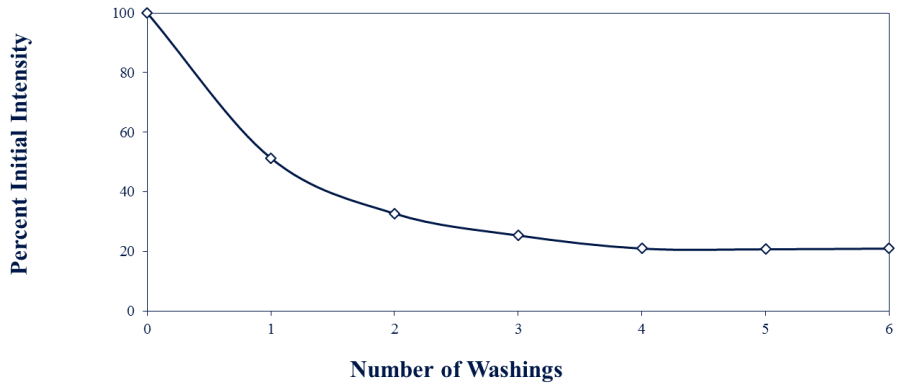

Figure 21: Results of the leaching tests with the DSA hydrogel expressed as percent initial intensity versus the number of washings.[27]

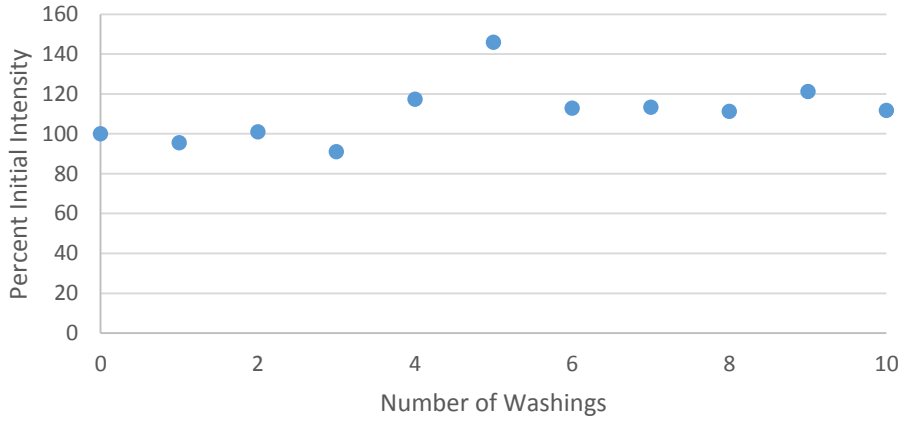

Figure 22: Results of the leaching tests with the compound **1** hydrogel expressed as percent initial intensity versus the number of washings.

Luminescent Transition Metal Complex

Synthesis of $[Os(CO)_2(sulf\text{-}dpp)Cl_2]$

Given the limitations of the smart hydrogel when applied to aqueous phase sensing, various TMCs were developed in order to be incorporated into luminescent MOFs. Based on the research performed by Amy Wagner, it was determined that

$[Os(CO)_2(sulf\text{-}dpp)Cl_2]$ was a viable TMC option given that the carbonyl ligands would raise the MLCT state, increasing the gap between the ground state and this transition, limiting the chance of the non-radiative processes significantly impacting the luminescence of the complex while also maintaining the emission wavelength within a range that is still optically useful. This complex was also chosen due to its large dipole moment. In order to successfully characterize the complex, it must be synthesized by first making the precursor $[Os(CO)_2Cl_2]$; the synthesis of this complex was undertaken due to limited supply.

The experimental IR spectrum for the produced $[Os(CO)_2Cl_2]$, prior to the recrystallization, is shown in Figure 23. There were two key peaks indicative of a carbonyl group at 2117.76 cm^{-1} and 2008.31 cm^{-1}, which are within experimental error of the literature values of 2120 cm^{-1} and 2012 cm^{-1}, respectively. This indicated that the product was the desired $[Os(CO)_2Cl_2]$, but the presence of smaller peaks that were possible impurities prompted the recrystallization of the product. After recrystallization, IR analysis was performed again. The resulting spectrum is shown in Figure 24. The carbonyl peaks were very close to the unpurified spectra. The values were 2118.28 cm^{-1} and 2024.60 cm^{-1}. Overall, the recrystallized product resulted in sharper, and more defined peaks, indicating an increase in purity. The mass of the product was 119.9 mg resulting in a percent yield of 40%, which was significantly lower than the reported 90% in the literature.[15] The lower yield obtained experimentally is most likely due to product loss upon purification, and the reaction might not have been run to completion. The low yield was also seen in the other two reactions; the second reaction afforded 18% yield

while the third only 16%. Given that the third reaction was stopped 24 h earlier than the others, it can be assumed that the low percent yield, as compared to the literature yield, is due to an incomplete reaction. However, since the second reaction only produced slightly more product than the third reaction, and it was allowed to reflux longer, it seems that a great deal of product is also lost upon recrystallization. It is also possible that the oil is not allowed enough time triturating, so it would be worth extending that time from 1 h to possibly 24 h in future syntheses.

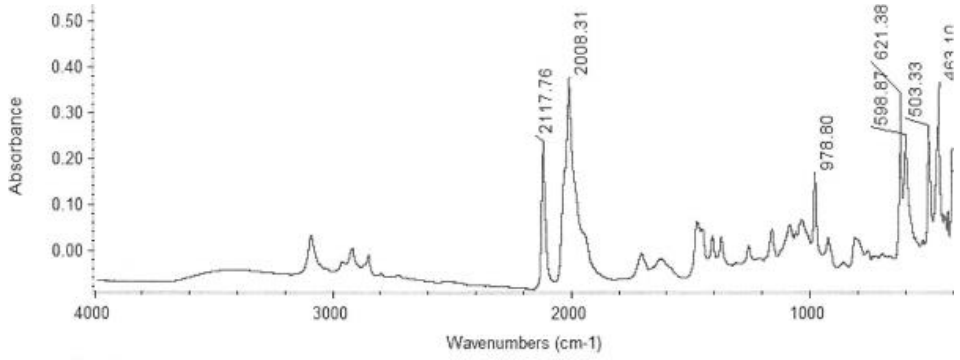

Figure 23: ATR-FTIR spectrum for unpurified $[Os(CO)_2Cl_2]$.

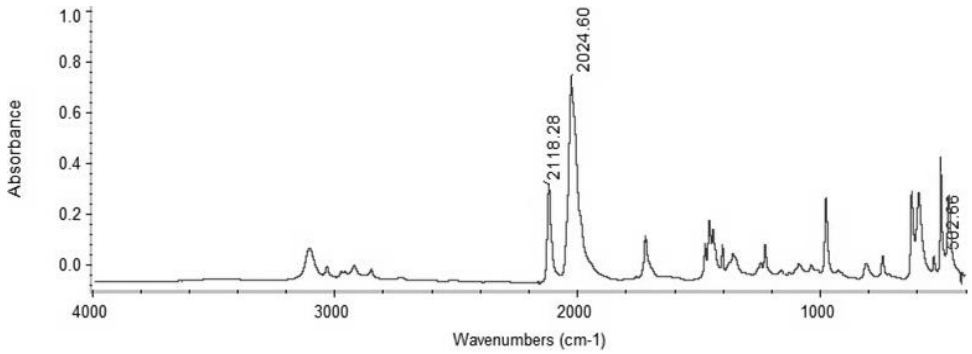

Figure 24: ATR-FTIR spectrum for recrystallized $[Os(CO)_2Cl_2]$.

The final $[Os(CO)_2(sulf\text{-}dpp)Cl_2]$ was then synthesized. The IR spectrum of this complex is shown in Figure 25. It was predicted that the success of the synthesis could be

determined based on the decrease in the signals at 2122 cm^{-1} and 2012 cm^{-1}, corresponding to the $[Os(CO)_2Cl_2]$ complex, and the increase in the signals at 2136 cm^{-1}, 2037 cm^{-1}, and 1960 cm^{-1}, corresponding to the desired $[Os(CO)_2(sulf\text{-}dpp)Cl_2]$ complex given that this method had be successful in the past.

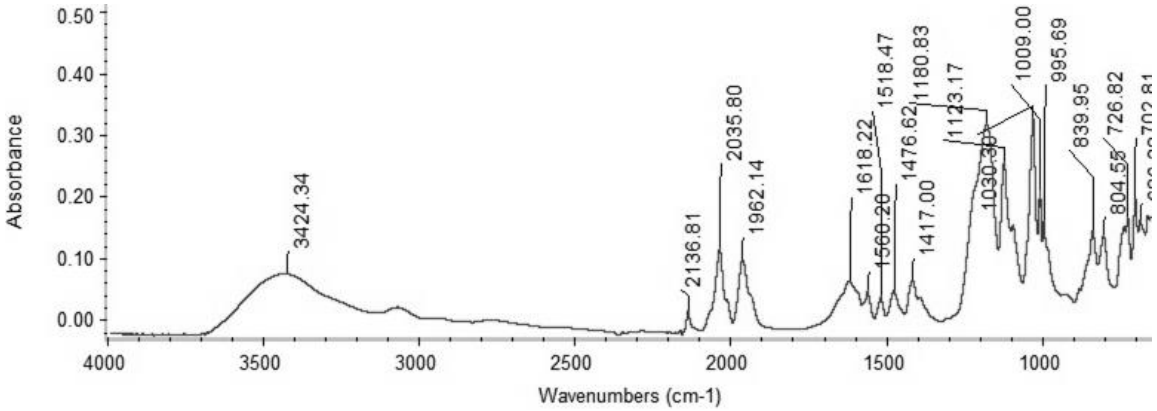

Figure 25: ATR-FTIR spectrum of the crude $[Os(CO)_2(sulf\text{-}dpp)Cl_2]$.

From the spectrum, it can be seen that $[Os(CO)_2(sulf\text{-}dpp)Cl_2]$ was successfully synthesized. The peaks corresponding to the precursor (2122 cm^{-1} and 2012 cm^{-1}) are no longer present while three new peaks appeared at 2136.81 cm^{-1}, 2035.80 cm^{-1}, and 1962.14 cm^{-1}. These three peaks are nearly identical to the signals identified by Amy at 2136 cm^{-1}, 2037 cm^{-1}, and 1960 cm^{-1}. The broad peak at 3424.34 cm^{-1} correspond to a water peak, indicating that the product was not pure, which can account for the large crude percent yield of 237%. A Sephadex G-50 column with methanol eluent should be used to purify the complex.

Quantum Yield Measurements: $[Ru(bpy)_3]Cl_2$, $[Ru(phen)_3]Cl_2$, and $[Os(CO)_2$(sulf-dpp)$Cl_2]$

In order to determine the feasibility for [Os(CO)2(sulf-dpp)Cl_2] to serve in a luminescence-based sensor, the quantum yield was determined. This was accomplished by determining the quantum yield of well-studied standards, in this case $[Ru(bpy)_3]Cl_2$ and $[Ru(phen)_3]Cl_2$, using the method established by Horiba and then using those quantum yields to determine the quantum yield of the osmium complex. It was predicted that the quantum yield of $[Os(CO)_2$(sulf-dpp)$]Cl_2$ would be smaller as compared to the ruthenium standards as a result of there being less available energy for emission due to the increase the gap between the MLCT state and ground state of the osmium atom compared to the energy distribution within the ruthenium atom.

The results from the absorbance measurements performed for standard solutions of $[Ru(bpy)_3]Cl_2$ and $[Ru(phen)_3]Cl_2$ showed a general trend of a maximum absorbance peak at 454 nm and 447 nm, respectively, indicating that these were the optimum excitation wavelengths for later fluorescence spectroscopy measurements. As expected, the order of increased absorbance correlated with the increase in concentration due to the presence of more molecules that absorb radiation around the optimum excitation wavelength. The Beer's Law plot for both sets of data, shown in Figure 26, indicated that the data did not deviate majorly from the line of best fit and is relatively precise since the R^2 value for $[Ru(bpy)_3]Cl_2$ is 0.999 while for $[Ru(phen)_3]Cl_2$ it is 0.996.

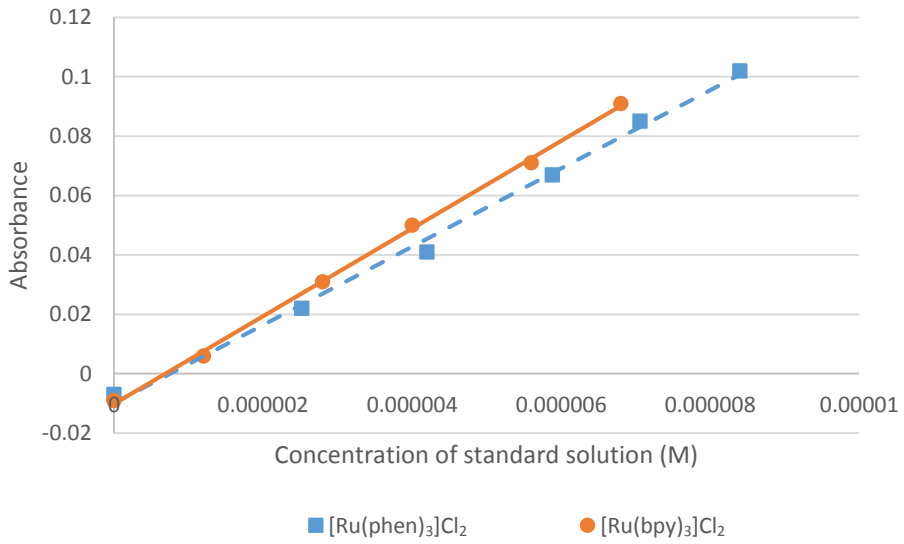

Figure 26: Beer's Law calibration curve for $[Ru(bpy)_3]Cl_2$ and $[Ru(phen)_3]Cl_2$.

The experimentally determined extinction coefficients for $[Ru(bpy)_3]Cl_2$ and $[Ru(phen)_3]Cl_2$ were 13200 ± 400 $Lmol^{-1}cm^{-1}$ (λ_{EX} = 454 nm) and 14700 ± 200 $Lmol^{-1}cm^{-1}$ (λ_{EX} = 447 nm), respectively. Neither of the experimentally determined molar extinction coefficients were within experimental error of the literature values: 14600 $Lmol^{-1}cm^{-1}$ for $[Ru(bpy)_3]Cl_2$ (λ_{EX} = 452 nm) and 18100 $Lmol^{-1}cm^{-1}$ for $[Ru(phen)_3]Cl_2$ (λ_{EX} = 447 nm). This deviation from the literature values is due in part to the fact that the absorption wavelength used for the $[Ru(bpy)_3]Cl_2$ measurements was not the one reported in the literature. However, the absorption wavelength did not deviate significantly from the literature wavelength, so the disagreement between the experimental and the literature molar extinction coefficients is more likely due to minor experimental errors in preparing the standard solutions and/or impurities in the commercially available standards. If the solution was actually a lower concentration, the slope of the Beer's Law plot would be

less than it should be, resulting in a smaller calculated molar extinction coefficient. Fortunately, the accuracy of the molar extinction coefficients does not matter for the purpose of the current work since the experimental absorbance of each solution is what is important in the analysis. For this reason, no additional efforts were made to improve accuracy.

Once the absorbance of each standard solution was determined, the emission of each was measured. This was accomplished by exciting each standard solution at its respective optimal excitation wavelength, which were mentioned previously. The data were collected with and without using polarizing filters. The filters were used in order to reduce the possible scattering from outside sources which limits the detection of the source radiation.

The emission and excitation data obtained for $[Ru(bpy)_3]Cl_2$ with and without polarizing filters were consistent with one another in that the overall trend seen without filters is still observed with filters, as shown in Figures 27 and 28. Figure 27 represents a consolidation of the emission spectra, while Figure 28 represents the excitation spectra of $[Ru(bpy)_3]Cl_2$. The emission spectra peaked at the varying wavelengths, 625 nm without polarizing filters and 605 nm with the filters, while the excitation spectra both had peaks at 450 nm. This difference between the observed emission maxima is not unexpected with the addition of the polarizing filters. The transmission efficiency of a grating monochromator depends upon the polarization of the light. Since the emission filter was oriented vertically, the spectra will shift to shorter wavelengths. This is because, for vertically polarized light, the transmission efficiency is greater at shorter wavelengths.[5]

The only other difference between each set of data is the intensity, with the data obtained without the filter having a higher intensity, which is expected.

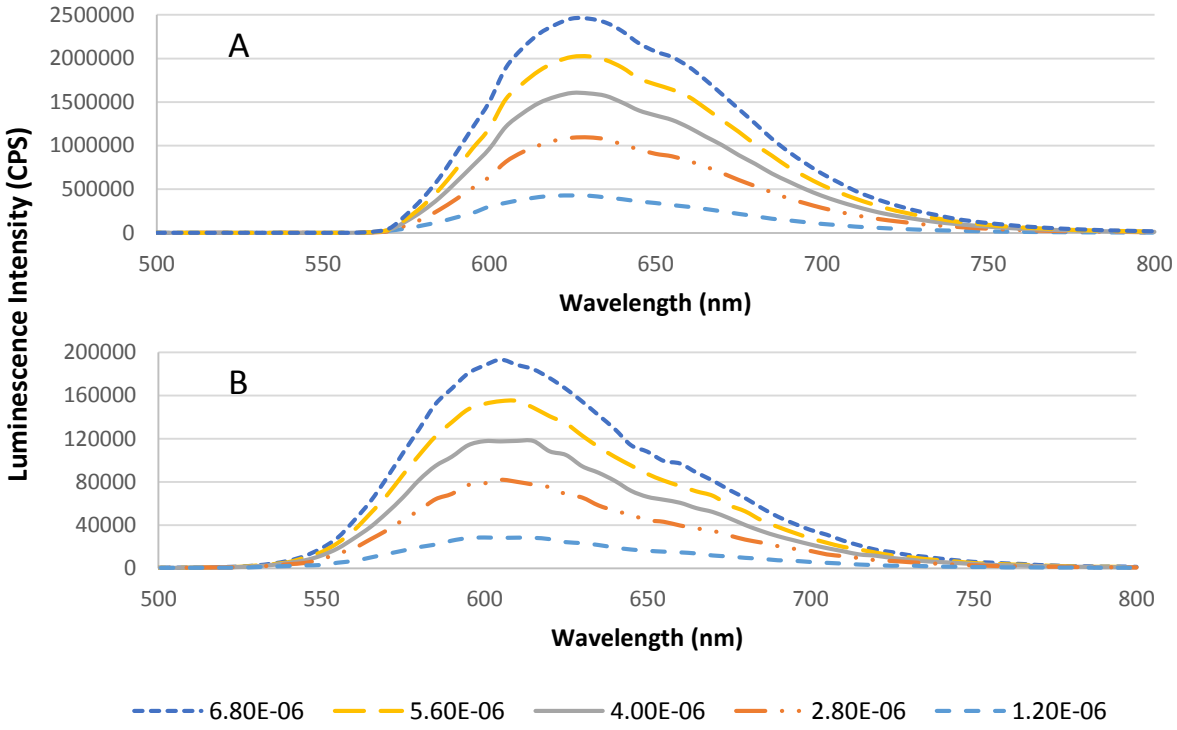

Figure 27: Consolidated emission spectra for $[Ru(bpy)_3]Cl_2$ A) without polarizing filters and B) with polarizing filters.

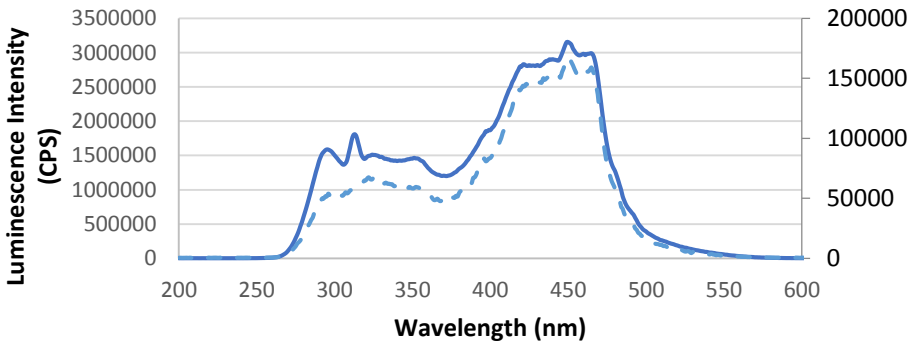

Figure 28: Excitation spectra for $[Ru(bpy)_3]Cl_2$ without polarizing filters (solid line) and with polarizing filters (dashed line).

The emission and excitation data obtained for $[Ru(phen)_3]Cl_2$ with and without polarizing filters were consistent with one another, as shown in Figures 29 and 30. Figure 29 represents a consolidation of the emission spectra, while Figure 30 represents the excitation data. The emission spectra peaked at the varying wavelengths, 616 nm without the filters and 590 nm with polarizing filters, and the excitation spectra both had peaks at 449 nm. This difference in emission maxima would be caused by the same phenomena causing the deviation in the $[Ru(bpy)_3]Cl_2$ data. The only other difference between each set of data is the intensity, with the data obtained without the filter having a higher intensity, which is expected.

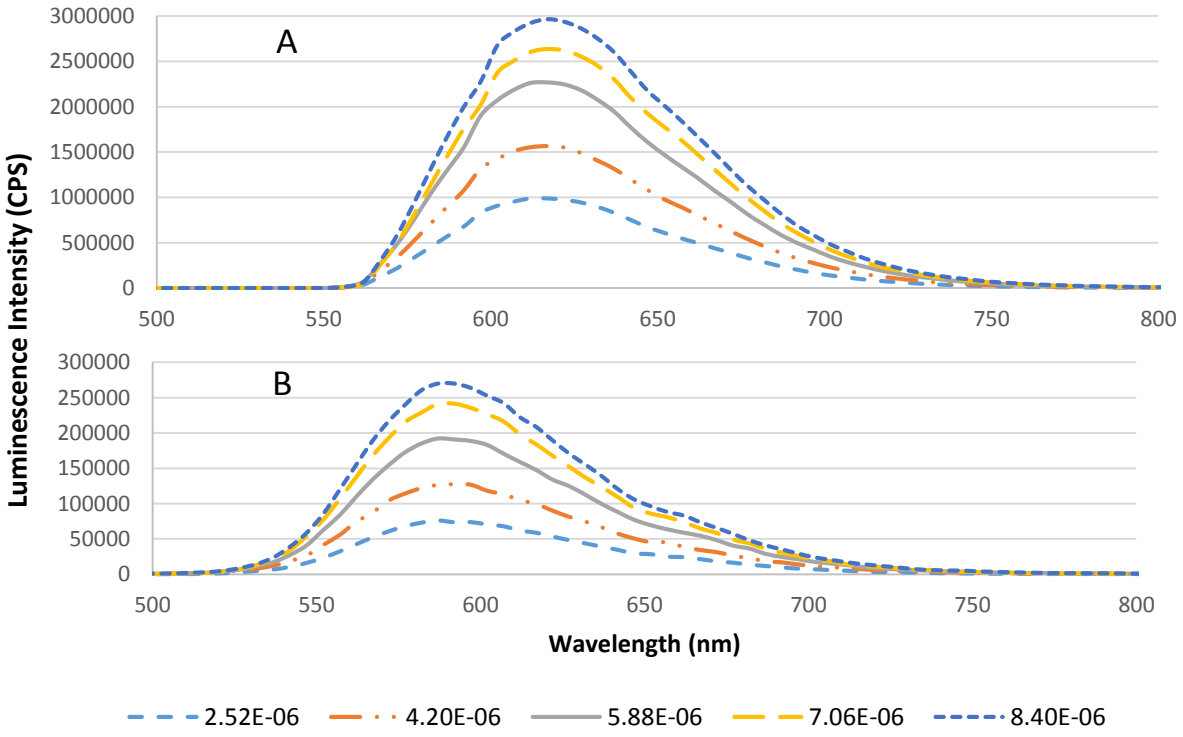

Figure 29: Consolidated emission spectra for $[Ru(phen)_3]Cl_2$ A) without polarizing filters and B) with polarizing filters.

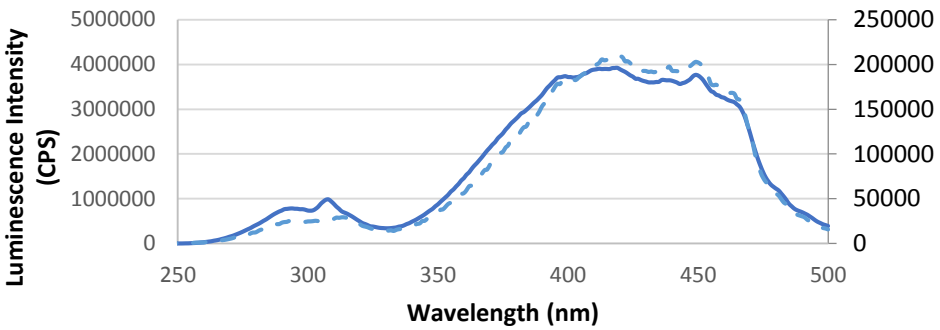

Figure 30: Consolidated excitation spectrum for $[Ru(bpy)_3]Cl_2$ without polarizing filters (solid line) and with polarizing filters (dashed line).

The emission data collected from both the $[Ru(bpy)_3]Cl_2$ and $[Ru(phen)_3]Cl_2$ standards were used to determine the quantum yield of each standard. A plot of the integrated intensity as a function of the absorbance of each standard solution is shown in Figure 31. The slope of each trend line displayed in Figure 31 and the literature values of the quantum yield of each complex[39] were substituted into Equation 1 in order to determine the experimental quantum yield of each standard solution relative to the other as the standard.[33] This calculation was performed for both data collected with and without the polarizing filters. Percent error was determined for the two quantum yields of each set of data relative to their individual literature values by substituting the literature and experimental quantum yields for a specific standard into the equation for percent error.

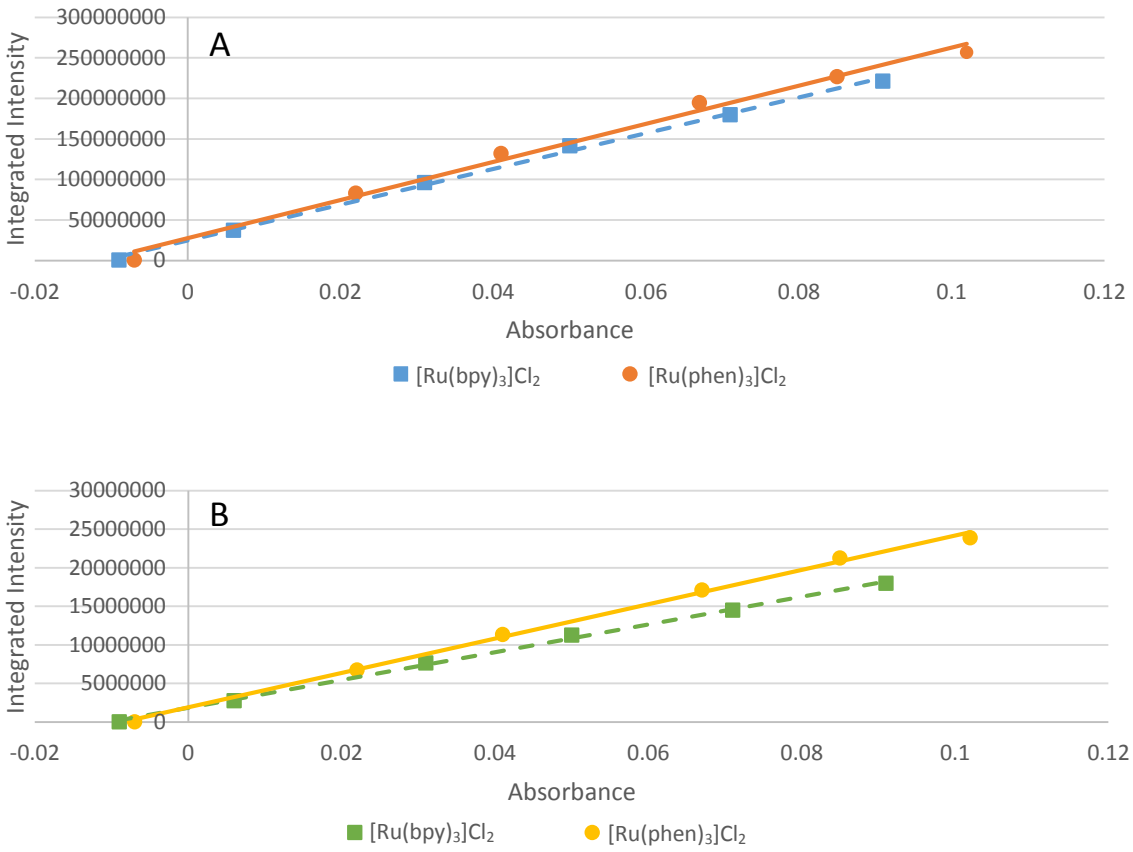

Figure 31: Integrated intensity of $[Ru(bpy)_3]Cl_2$ and $[Ru(phen)_3]Cl_2$ as a function of absorbance A) with polarizing filters and B) without polarizing filters.

The gradients for each line of best fit for the data obtained without filters are within experimental error of one another; the $[Ru(bpy)_3]Cl_2$ data produced a gradient of $(2.21 \pm 0.05) \times 10^9$ and the $[Ru(phen)_3]Cl_2$ data produced a gradient of $(2.30 \pm 0.10) \times 10^9$. The gradients for each line of best fit for the data obtained with filters, however, are not within experimental error of one another; the $[Ru(bpy)_3]Cl_2$ data produced a gradient of $(1.800 \pm 0.040) \times 10^8$ and the $[Ru(phen)_3]Cl_2$ data produced a gradient of $(2.23 \pm 0.06) \times 10^8$.

In calculating the quantum yield of both $[Ru(bpy)_3]Cl_2$ and $[Ru(phen)_3]Cl_2$ the second term of Equation 1 was ignored since both standards were prepared in water, which has a refractive index of 1.33 at room temperature. The quantum yields for $[Ru(bpy)_3]Cl_2$ and $[Ru(phen)_3]Cl_2$, with and without polarizing filters, can be seen in Table 3 along with the respective literature values.

Table 3: Experimental and literature quantum yields for $[Ru(bpy)_3]Cl_2$ and $[Ru(phen)_3]Cl_2$.

	$[Ru(bpy)_3]Cl_2$			$[Ru(phen)_3]Cl_2$		
	Experimental ϕ	Literature ϕ	% Difference	Experimental ϕ	Literature ϕ	% Difference
With filter	0.0259 ± 0.0008	0.028	7.5%	0.035 ± 0.001	0.032	8.1%
Without filter	0.030 ± 0.002		7.2%	0.030 ± 0.002		6.7%

Since the percent differences for each of the two quantum yields for the standards fell within 10% experimental error, the differences are deemed acceptable, according to the literature method, and can be used in determining the quantum yield of $[Os(CO)_2(sulf\text{-}dpp)Cl_2]$. It is ideal to use the quantum yields determined from the data collected with the filters since these quantum yields have better precision compared to the quantum yields determined from the data collected without filters. However, since the osmium complex did not produce enough signal to warrant the use of the filters, the quantum yields calculated from the data collected without the filters were used.

The quantum yield measurements for $[Os(CO)_2(sulf\text{-}dpp)Cl_2]$ were performed in the same manner as the ones for the two ruthenium standards. Absorbance was measured for solutions of different concentration and emission was measured at the optimal

excitation wavelength as determined by the absorbance spectra. The results from the absorption data of $[Os(CO)_2(sulf\text{-}dpp)Cl_2]$ is shown in a Beer's Law plot (Figure 32).

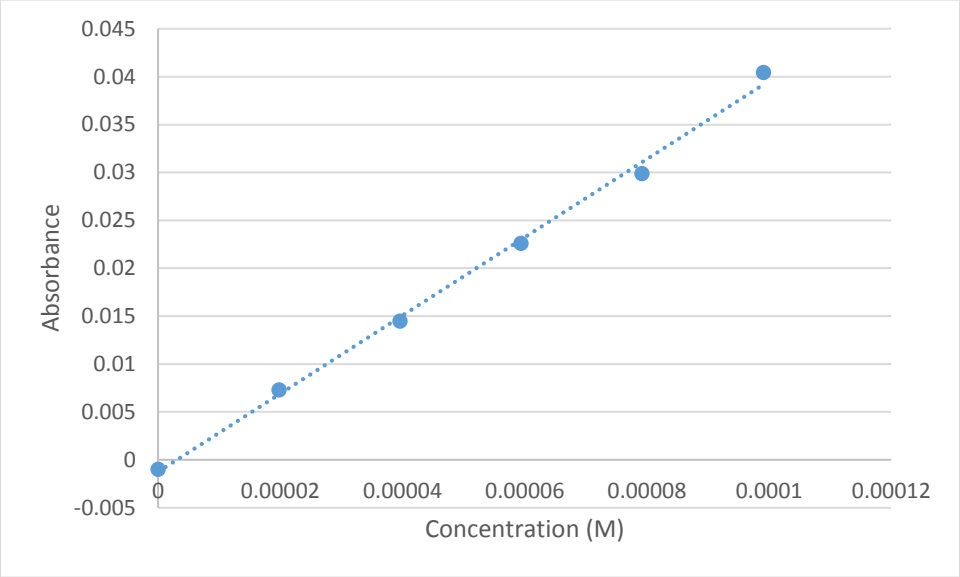

Figure 32: Beer's Law calibration curve for $[Os(CO)_2(sulf\text{-}dpp)Cl_2]$.

Overall, the absorption data of the $[Os(CO)_2(sulf\text{-}dpp)Cl_2]$ solutions showed a general trend of a maximum absorbance peak at 500 nm, indicating that this was the optimum excitation wavelengths for later fluorescence spectroscopy measurements. As expected, the order of increased absorbance correlated with the increase in concentration due to the presence of more molecules that absorb radiation around the optimum excitation wavelength. The Beer's Law plot for the data set indicated that the data did not deviate significantly from the line of best fit and is relatively precise since the R^2 value is 0.997. The experimentally determined extinction coefficients for $[Os(CO)_2(sulf\text{-}dpp)Cl_2]$ was 410 ± 10 $L \cdot mol^{-1}cm^{-1}$ (λ_{EX} = 500 nm). This extinction coefficient is much lower than that of either of the ruthenium complexes chosen as standards, indicating that

a higher concentration of the osmium complex will be needed in order to obtain a signal comparable to that of a ruthenium complex.

The results of the absorption measurements were then used in the emission characterization of the osmium complex. Since osmium complexes emit at lower intensities compared to their ruthenium counterparts, both emission and excitation measurements were performed without the use of the polarizing filters. The emission and excitation data obtained for $[Os(CO_2)_2(sulf\text{-}dpp)]Cl_2$ without polarizing filters are shown in Figures 33 and 34. Figure 33 represents the emission spectra of all the concentrations of the $[Os(CO_2)_2(sulf\text{-}dpp)]Cl_2$ solution, while Figure 34 represents the excitation data. The emission spectra peaked at a wavelength of 710 nm and the excitation spectrum had a peak at 400 nm.

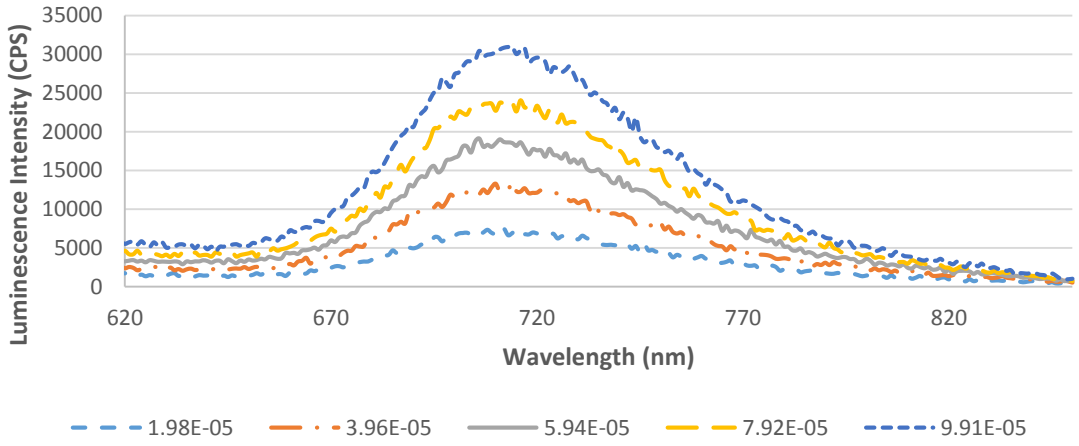

Figure 33: Emission spectra for $[Os(CO_2)_2(sulf\text{-}dpp)]Cl_2$ without polarizing filters.

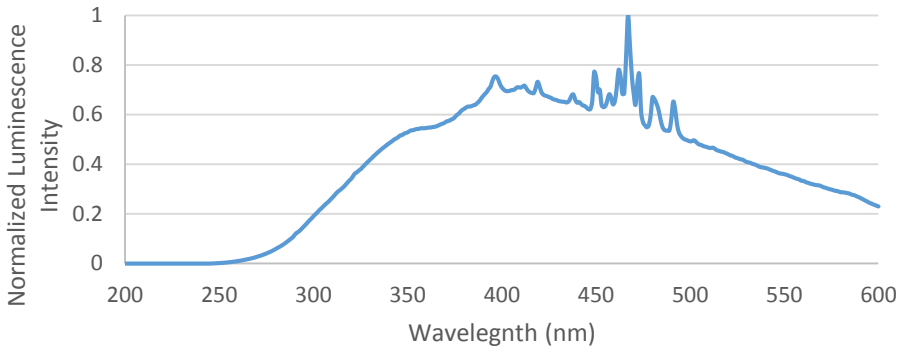

Figure 34: Excitation spectrum for $[Os(CO_2)_2(sulf\text{-}dpp)]Cl_2$ without polarizing filters.

The emission data collected from the $[Os(CO_2)_2(sulf\text{-}dpp)]Cl_2$ solutions was used to determine the quantum yield of the complex. A plot of the integrated intensity as a function of the absorbance of each standard solution is shown in Figure 35. The slope of the line of best fit displayed in Figure 35 and the quantum yield of the complex, as determined by one of the standards, were substituted into Equation 1 in order to determine the experimental quantum yield of the complex relative to the other standard.[27] This calculation was performed using each of the two standard ruthenium complexes as the standard within the equation. Percent error was determined for the two quantum yields via the same method used for the ruthenium complexes.

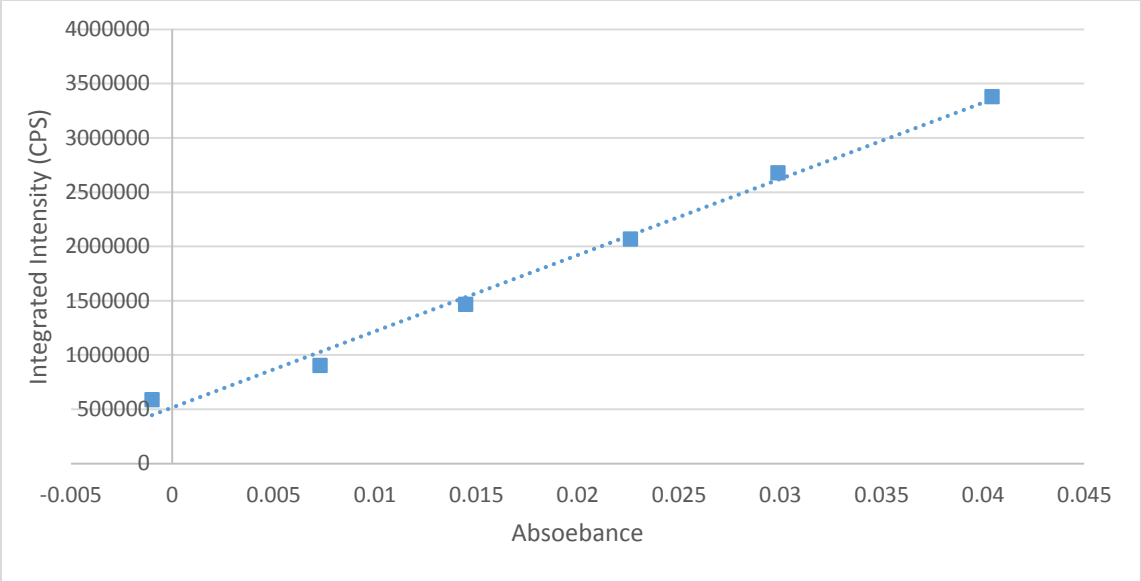

Figure 35: Integrated intensity of $[Os(CO_2)_2(sulf\text{-}dpp)]Cl_2$ as a function of absorbance without polarizing filters.

The gradients for the line of best fit for the data obtained for $[Os(CO_2)_2(sulf\text{-}dpp)]Cl_2$, without the use of filters is $(5.30 \pm 0.20) \times 10^7$. In calculating the quantum yield of the osmium complex with respect to each of the standards, the second term of Equation 1 was ignored since all three standards were prepared in water, which has a refractive index of 1.33 at room temperature. The quantum yields determined for $[Os(CO_2)_2(sulf\text{-}dpp)]Cl_2$ were 0.00089 ± 0.00006 with a percent difference of 6.7% when $[Ru(bpy)_3]Cl_2$ was the standard and 0.00095 ± 0.00006 with a percent difference of 7.2% when $[Ru(phen)_3]Cl_2$ was the standard. Since the percent differences for the two quantum yields of the osmium complex fell within 10% experimental error, the differences are deemed acceptable, according to the literature method. The mean quantum yield is 0.00092 ± 0.00006. This quantum yield value is two orders of magnitude lower than that of either standard ruthenium complex indicating, again, that a higher concentration of the

osmium complex is required in order to obtain an appreciable signal for sensing as compared to the concentration of a ruthenium complex required in order to obtain the same signal. However, the calculated quantum yield is comparable to the quantum yield of other osmium complexes, which have found use in sensing applications.[39] When incorporated into a MOF, the concentration of $[Os(CO_2)_2(sulf\text{-}dpp)]Cl_2$ should increase enough to afford an appreciable signal.

Conclusion & Future Work

Existing luminescence-based sensing techniques exploit one sensor molecule for one analyte, resulting in the need to synthesize a different sensor molecules for each new analtye. Attempts at the design and creation of a sensor that has a smart hydrogel in which an environment-sensitive luminescent reporter molecule is embedded were successful in gas phase sensing of relative humidity, but had limited success with repeated use in aqueous phase sensing of lactate due to the leaching of the fluorophore. This body of work sought to characterize two compounds designed as a response to this limitation and evaluate their applicability as reporter molecules for their respective sensor matrices.

The first compound investigated was a nitrile DSA derivative (compound **1**) that was designed to polymerize into the hydrogel itself to eliminate the chance of leaching once the gel is introduced to an aqueous environment. The derivative showed reasonable, but complex, solvent sensitivity when exposed to solvent environments of varying

polarities. Once polymerized into the hydrogel, two possible outcomes were predicted: 1) compound **1** would experience a greater sensitivity to the introduction of the analyte given that it would be exposed to a mostly hydrophobic environment until water entered due to the swelling of the gel; 2) compound **1** would lose sensitivity due to a greater hindrance of the formation of a TICT state caused by its incorporation into the gel itself. In order to determine the effect the polymerization into the hydrogel had on the nitrile derivate, the humidity sensitivity of this gel was then explored by exposing the gel to a range of relative humidity levels (0% to 75%) and then the response of the fluorophore was examined. It was determined that the fluorophore lost its sensitivity when incorporated into the hydrogel based on the constant position of the emission maximum for the gel in each level of humidity, but it is not clear whether or not this is a consequence of a hindered TICT.

However, it was proposed that the hydrogel could be utilized as a relative intensity ratio sensor given that, when excited at 323 nm, the gel exhibited a narrowing of the present peak with an increase in the relative humidity. This option should be explored more in depth by the characterization of other gel films since each could possibly exhibit differences in their responses. Low temperature measurements should also be performed on the gels in order to better characterize the two excited states observed in this body of work. These measurements would assist in lessening the complications of the characterization experienced at room temperature.

The gel was also tested to ensure that the addition of the acrylamide group did result in the fluorescent reporter being polymerized into the hydrogel. The results of this

test suggested that **1** did polymerize into the hydrogel like it was designed to do. It would also be advantageous to ensure that the DSA derivative was actually uniformly distributed throughout the polymer. This would be accomplished through the use of a black light. If compound **1** was evenly distributed throughout the hydrogel, fluorescent yellow dots should be observed uniformly throughout the microscope slide and not clustered in one section of the slide.

Given that the derivative synthesized by Diwu exhibited similar solvent sensitivity, even with the electronic of the molecule being reverse of DSA, it would be advantageous to attach an acrylamide group and execute the same line of testing performed on compound **1**. It would be interesting to determine if this derivative would also experience hindered formation of the TICT state and if it would result in a better reporter molecule overall. Since the Diwu derivative exhibited larger Stokes shift and better consistency in the increase of those shifts with the increase in solvent polarity on average, it is possible that reversing the electronic of the original DSA molecule actually improves its ability to be used as a luminescent reporter molecule in a sensing matrix.

The second response to limit the leaching observed within the previous hydrogel used for relative humidity sensing was to eliminate the gel as the sensor matrix entirely and develop a MOF with a luminescent TMC as the reporter molecule. The complex characterized was $[Os(CO_2)_2(sulf\text{-}dpp)]Cl_2$ which was determined to be a possible structure for use within a MOF by previous studies. Both the experimental molar extinction coefficient (410 ± 10 $Lmol^{-1}cm^{-1}$) and quantum yield (0.00092 ± 0.00006) measurements determined that this complex would require a much higher concentration

in order to be a comparable option as luminescent reporter molecule compared to available ruthenium complexes due to the low values calculated. Once incorporated into a MOF, the signal obtained should be more appreciable given the increase in TMC concentration. Due to rigidochromic effects, the quantum yield should also increase due to the increase of the rigidity of the complex. Low temperature measurements should also be performed for the quantum yield measurements of $[Os(CO_2)_2(sulf\text{-}dpp)]Cl_2$. This would limit the interference of competing nonradiative processes that can cause lower emission intensity of the higher energy excited state to be observed, lessening the magnitude of the quantum yield of the complex.

1. Harris, D. C. *Quantitative Chemical Analysis*, 8th ed.; W.H. Freeman and Company: New York, 2010, pp 408-414.

2. Kickler, T. Clinical Analyzers. Advances in Automated Cell Counting. *Anal. Chem.*, **1999**, *71*, 363R.

3. Davalos, A.; Gomez-Cordoves, C.; Bartolome, B. Extending Applicability of the Oxygen Radical Absorbance Capacity (Orac-Fluorescein) Assay. *J. Agric. Food Chem.*, **2004**, *52*, 48.

4. Hanson, F.; Hanson, B. Fluorescence Probes for Celluar Assays. *Com. Chem. High. T. Scr.*, **2008**, *11*, 505.

5. Lakowicz, J. R. Introduction to Fluorescence & Solvent and Environmental Effects. In *Principles of Fluorescence Spectroscopy*, 3rd ed.; Springer: Singapore, 2006, pp 9-12 & pp 205-208.

6.Collingridge, D. R.; Young, W. K.; Vojnovic, B.; Wardman, P.; Lynch, E. M.; Hill, S. A.; and Chaplin, D. J. *Radiation Research*, **1997**, *147*, 329.

7. Alaoui, I.M. Applications of Luminescence to Fingerprints and Trace Explosives Detection. In *Unexpected Ordnance Detection and Mitigation*; Springer: Netherlands, 2009, pp 189-196.

8. Toal, S. J.; Trogler, W. C. Polymer Sensors for Nitroaromatic Explosives Detection. *J. Master Chem.*, **2006**, *16*, 2871.

9. Toal, S. J.; Sanchez, J. C.; Dugan, R. E.; Trogler, W. C. Visual Detection of Trace Nitroaromatic Explosive Residue Using Photoluminescent Metallole-Containing Polymers. *J. Forensic Sci.*, **2007**, *52*, 79.

10. Kneas, K. A.; Xu, W.; Demas, J. N.; DeGraff, B. A. Oxygen Sensors Based on Luminescence Quenching: Interactions of Tris(4,7-Diphenyl-1,10-Phenanthroline)Ruthenium(II) Chlorides and Pyrene with Polymer Supports. *Appl. Spectrosc.*, **1997**, *51*, 1346.

11. Demas, J. N.; DeGraff, B. A.; Coleman, P. B. Oxygen Sensors Based on Luminescence Quenching. *Anal. Chem.*, **1999**, *71*, 793.

12. Carraway, E.; Demas, J. N.: DeGraff, B. A.; Bacon, D. R. Photophysics and Photochemistry of Oxygen Sensors Based on Luminescent Transition-Metal Complexes. *Anal. Chem.*, **1991**, *63*, 337.

13. Kneas, K. A.; Xu, W.; Demas, J. N.; DeGraff, B. A., Dramatic Demonstration of Oxygen Sensing by Luminescence Quenching. *J. Chem. Ed.*, **1997**, *74*, 696.

14. Xu, W.; Wittich, F.; Banks, N.; Zink, J.; Demas, J. N.; DeGraff, B. A. Quenching of Luminescent Ruthenium(II) Complexes by Water and Polymer-Based Relative Humidity Sensors. *Appl. Spectrosc.*, **2007**, *61*, 1238.

15. Bedoya, M.; Diez, M. T.; Moreno-Bondi, M. C.; Orellana, G. Humidity Sensing with a Luminescent Ru(II) Complex and Phase-Sensitive Detection. *Sens. Act. B*, **2006**, *113*, 573.

16. Demas, J. N.; DeGraff, B. A. Design and Application of Highly Luminescent Transition Metal Complexes. *Anal. Chem.*, **1991**, *63*, 829A.

17. Van Slageren, J.; Stufkens, D. J. Tuning the Excited-State Properties of $[M(SnR_3)_2(CO)_2(\alpha\text{-diimine})]$ (M = Ru, Os; R = Me, Ph). *Inorg. Chem.*, **2001**, *40*, 277.

18. Baca, S. G.; Adams, H.; Grange, C. S.; Smith, A. P.; Saranovich, I.; Ward, M. D. $[Os(bipy)(CN)_4]^{2-}$ and Its Relatives as Components of Polynuclear Assemblies: Structural and Photophysical Properties. *Inorg. Chem.*, **2007**, *46*, 9779.

19. Xu, W.; Kneas, K. A.; Demas, J. N.; DeGraff, B. A. Oxygen Sensors Based on Luminescence Quenching of Metal Complexes: Osmium Complexes Suitable for Laser Diode Excitation. *Anal. Chem.*, **1996**, *68*, 2605.

20. Erten-Ela, S.; Colak, S. G.; Ocakoglu, K. The first application of water-soluble ruthenium phenanthroline complex for dye sensitized solar cells from aqueous solution using PEDOT:PSS counter electrode versus platinum counter electrode. *Inorganica Chimica Acta*, **2013**, *405*, 252.

21. Liu, C.; Chen, W.; Shi, W.; Peng, B.; Zhao, Y.; Ma, H.; Xian, M. Rational Design and Bioimaging Applications of Highly Selective Fluorescence Probes for Hydrogen Polysulfides. *J. Am. Chem. Soc.,* **2014**, *136*, 7257.

22. Wu, Y.; Zheng, W.; Qu, J. Y. Sensing Cell Metabolism by Time-Resolved Autofluorescence. *Opt. Lett.,* **2006**, *31*, 3122.

23. Moore, S. A.; Frazier, S. M.; Sibbald, M. S.; DeGraff, B. A.; Demas, J. N. On the causes of altered photophysics of luminescent metal complexes embedded in polymer hosts. *Langmuir*, **2001**, *27*, 9567.

24. Narayanaswamy, R.; Wolfbeis, O. S., *Optical Sensors.* Springer: Berlin, 2004.

25. Otsuki, S.; Adachi, K. Effect of Humidity on the Fluorescence Properties of a Medium-Sensitive Fluorophore in a Hydrophilic Polymer Film. *Photochem. Photobiol. A: Chem.*, **1993**, *71*, 169.

26. Otsuki, S.; Adachi, K. Medium-Sensitive Fluorophore as a Moisture Probe in Polymer Film. *Polymer J.,* **1994**, *26*, 343.

27. Tellis, J. C.; Strulson, C. A.; Myers, M. M.; Kneas, K. A. Relative Humidity Sensors Based on an Environment-Sensitive Fluorophores in Hydrogel Films. *Anal. Chem.,* **2011**, *83*, 928.

28. Ebara, M.; Kotsuchibashi, Y.; Narain, R.; Idota, N.; Kim, Y. J.; Hoffman, J. M.; Uto, K.; Aoyagi, T. Smart Hydrogels. In *Smart Biomaterials*; Springer: Berlin, 2014.

29. Cerón-Carrasco, J. P.; Jacquemin, D.; Laurence, C.; Planchat, A.; Reichardt, C.; Sraïdi, K. Solvent polarity scales: determination of new $E_T(30)$ values for 84 organic solvents. *J. Phys. Org. Chem.,* **2014**, *27*, 512.

30. Diwu, Z.; Lu, Y.; Zhang, C.; Klaubert, D.; Haugland, R. P. Fluorescent Molecular Probes II. The Synthesis, Spectral Properties and Use of Fluorescent Solvatochromic Daproxyl™ Dyes. *Photochemistry and Photobiology*, **1997**, *66*, 424.

31. Jobin Yvon Horiba. *A Guide to Recording Fluorescence Quantum Yields*; Jobin Yvon Ltd.: United Kingdom.

32. Aly, S. M.; Carraher, C. E.; Harvey, P. D. Introduction to Photophysics and Photochemistry. *CQMF*, **2014**, 1-64.

33. Milgrom, L. R. The Porphyrins. In *The Colours of Life: An Introduction to the Chemistry of Porphyrins and Related Compounds*; Academic Press: New York, 1978.

34. Abdel-Kader, M. H., Fundamentals of Photophysics, Photochemistry, and Photobiology. In *Photodynamic Therapy*; Springer: Berlin, 2014; pp 25-58.

35. Abdel-Kader, M. H., Fundamentals of Photophysics, Photochemistry, and Photobiology. In *Photodynamic Therapy*; Springer: Berlin, 2014; pp 25-58.

36. American Society for Photobiology. Basic Photophysics. http://www.photobiology.info/Visser-Rolinski.html#TOP (accessed Sep 2015).

37. Verhoeven, J. W. Glossary of terms used in photochemistry (IUPAC Recommendations 1996). *Pure and Applied Chemistry*, **2009**, *68*, 2223.

38. Greenspan, L. *J. Res. Nat. Bur. Stand. A*, **1977**, *81*, 89.

39. Montalti, M.; Credi, A.; Prodi, L.; Gandolfi, M. T. Photophysical Properties of Transition Metal Complexes. In *Handbook of Photochemistry*, 3rd ed.; CRC Press: New York, 2006, pp 392-398.